minerals

MDPI

Article

Age and Origin of the Massangana Intrusive Suite and Associated Mineralizations, in the Rondônia Tin Province: Petrography, U-Pb, and Lu-Hf Isotopes Zircons

Beatriz Pereira Debowski [1], Guilherme Loriato Potratz [1], Armando Dias Tavares Júnior [2], Maria Virgínia Alves Martins [1,3] and Mauro Cesar Geraldes [1,*]

[1] Faculdade de Geologia, Departamento de Mineralogia e Petrologia Ígnea (DMPI), Universidade do Estado do Rio de Janeiro (UERJ), Rua São Francisco Xavier, 524—Bloco A, Rio de Janeiro 20550-013, Brazil
[2] Instituto de Física, Universidade do Estado do Rio de Janeiro (UERJ), Rua São Francisco Xavier, 524, Bloco D, Rio de Janeiro 20550-900, Brazil
[3] Departamento de Geociências, GeoBioTec, Universidade de Aveiro, 3810-193 Aveiro, Portugal
* Correspondence: geraldes@uerj.br

Abstract: Rondônia intrusive suites represent the youngest A-type magmatism that occurred in the SW of the Amazon craton, with mineralizations in Sn, Nb, Ta, W, and topaz. Petrological and isotopic studies (U-Pb and Lu-Hf by LA-ICP-MS) allowed the Massangana granite to be subdivided into São Domingos facies (medium to fine biotite-granite), Bom Jardim facies (fine granite), Massangana facies (pyterlites and coarse granites) and Taboca facies (fine granites). The crystallization ages obtained were between 995.7 ± 9.5 Ma to 1026 ± 16 Ma, and the εHf values vary significantly between positive and negative, showing predominantly crustal sources for forming these rocks. Petrographic studies on ore samples indicate the action of co-magmatic hydrothermal fluids enriched in CO_2, H_2O, and F. These ores are characterized by endogreisens, exogreisens, pegmatites, and quartz veins that are explored in the São Domingos facies area. The endogreisens and exogreisens are formed by topaz-granites and zinnwaldite-granites; the pegmatites are formed by topaz-zinnwaldite-cassiterite-granites; and the veins by cassiterite-sulfides and quartz. The geometries of the mineralized bodies indicate a dome-shaped contact with the host rocks in the magma chamber and can be attributed to residual accumulation. In this sense, the origin of these ores is related to the evolution of intrusive granitic bodies where the terminal phases of the fluid-enriched magma are lodged in the apical portions, and the origin of the mineralized bodies present a biotite-granite, albite-granite, and endogreisens evolution (potassium series), or biotite-granite, alkali-granite and endogreisens (sodic series) and these rocks present TDM ages that indicate a concerning relation to the non-mineralized rocks of Massangana granite.

Keywords: Rondônia Tin Province; U-Pb; Lu-Hf; LA-ICP-MS; Mesoproterozoic; Neoproterozoic; Brazil

Citation: Debowski, B.P.; Potratz, G.L.; Tavares Júnior, A.D.; Alves Martins, M.V.; Geraldes, M.C. Age and Origin of the Massangana Intrusive Suite and Associated Mineralizations, in the Rondônia Tin Province: Petrography, U-Pb, and Lu-Hf Isotopes Zircons. *Minerals* **2022**, *12*, 1304. https://doi.org/10.3390/min12101304

Academic Editor: Jane H. Scarrow

Received: 20 August 2022
Accepted: 21 September 2022
Published: 16 October 2022

1. Introduction

The study of granitic rocks is significant for understanding the formation of Earth planet and for understanding the formation of metallic deposits. This is because granites are the most abundant rocks in the upper continental crust and hold essential information about the evolution of the Planet. The generation of granites is a phenomenon related, primarily, to continents, and the calc-alkaline series occur essentially in orogenetic regions and transitional environments. In contrast, the type-A granites are typical of intra-plate environments. The orogenic granites show variations even during orogenic magmatism due to the position of magmas generation, as suggested by [1]. Thus, the plutonic manifestations located near the subduction zone are characterized by K-poor mineralogy, resulting

in compositions between calcium-alkaline and trondhjemitic. Advancing towards the continent, the amount of potassium increases, thus appearing in the calc-alkaline, granodioritic, and monzonitic series. Alkaline granites occur even further away from the subduction line, related to rift zones.

Most felsic or granitic magmas are derived from the partial melting of predominantly crustal material, however granitic melts produced by the differentiation of more mafic magmas in an oceanic environment can occur, as occurs at the Mid-Atlantic Ridge in Iceland, where eruptions of the Hekla volcano are initiated by a pulse of felsic ash rapidly followed by eruptions of typically more basaltic andesites. Nowadays, it is a consensus in the literature that andesitic magmas from a subduction environment receive both contributions from the continental crust and the lithospheric mantle, which, through mixing and fractional crystallization processes, result in suites of calc-alkaline composition [1,2].

Reduced A-type magmas, also called ilmenite-series magmas, are related to a quartz-feldspathic igneous source, probably with a metasedimentary component [3], or differentiation from a tholeiitic source [4]. Oxidized A-type magmas, or magnetite-series magmas, are derived from fluids with considerable amounts of water ($\geq$4 wt.%), originating from a quartz-feldspathic source in the lower crust under oxidizing conditions. Ref. [5] proposed that ferroan granites could form in three ways: (1) from partial melting of a quartz-feldspathic crust [6,7], (2) from basaltic magmas differentiation [6], or (3) from a combination of these two processes, through magmatic mixing and/or fractional crystallization with host assimilation, also defined as AFC [8,9].

Refs. [10–12] discussed the relevance of the current use of the term A-type granites and referred to the absence of a genetic classification scheme. The authors observed that the crust cut by A-type granites does not show significant changes related to magma composition in modal terms and major elements, but is marked by changes in isotopic and trace elements composition. According to [13], the characteristics of A-type granites are related to the heterogeneity of the crust sources. These authors associate the great variety of isotopic signatures found in suites of A-type granites with magmas of contrasting compositions added to small degrees of partial melting with the generation of small volumes of primary magmas.

The A-type granites described by [14,15] had very different characteristics from those classified as I-type and S-type, such as an intercontinental environment, high concentrations of Fe/(Fe + Mg), K_2O, and K_2O/Na_2O, low levels of CaO and MgO, in addition to high concentrations of incompatible trace elements, such as REE, Zr, Nb and Ta and low concentration of compatible trace elements in mafic silicates and feldspars. The work of [10] became a benchmark in the classification of granites. From this work, several authors started to use the term frequently, and several granitic suites worldwide were classified as A-type, such as the Pikes Peak Batholith in the White Mountain magmatic series in New Hampshire, the Young Granites of Nigeria, the Greenland Gardar Province, among others.

The Rondônia Tin Province is an example of rapakivi granites related to tin ore deposits. It has been studied for at least 50 years [16–21]; however, there are still gaps to be filled, such as the source of the magma that resulted in the formation of these rocks and the relationship of these with mineralization.

2. Mineralization Associated with Type-A Granites

An exciting feature observed by researchers of the granitic series [7,22–26] is the nature of the metallic assemblage of mineral deposits genetically associated with granitic intrusions, which is generally controlled by the origin and composition of the generating magma. It carries the metals that were indeed donated to the rock that first melted, that is, the protolith. When a felsic magma is derived from sedimentary rocks, mineral associations are characterized by the concentration of metals, such as Sn, W, U, and Th; when the protolith is an ancient igneous rock (I-type granite), the mineral association is typical and has incompatible elements, such as Li, Be, and metals such as Cu, Mo, Pb, Zn and Au [27], volatiles (F and Cl) and water amid alkaline, acidic and low viscosity

magma. Associated with this type of residual magmatic fluid, the end product of the magmatic differentiation process remains in a certain equilibrium until regional or local tectonic disturbances generate faults and/or fractures that allow its percolation. When depressurized, this fluid percolation occurs between faults and fractures, interacting with the host rocks (granites and gneisses) and modifying its mineralogy, which results in the formation of endo and exogreisens; as well as quartz veins containing or not disseminated ore and pegmatitic veins [28,29].

Rapakivi *sensu lato* granites comprise both anorogenic and orogenic granites, do not have any age-limiting factors, and only characterize granitic rocks with K-feldspar held by plagioclase oval. According to [30], the rapakivi texture is described: (1) by the shape of K-feldspar phenocrysts; (2) by feldspars covered by thin oligoclase-andesine; (3) occurrence of two generations of K-feldspar and quartz. Studies carried out on oval K-feldspars from the Wiborg rapakivi granite batholith of SE Finland [26,30] indicated that the oligoclase rings present higher values of $\delta^{18}O$ and $^{87}Sr/^{86}Sr$ than the host K-feldspar, indicating the presence of a low-temperature late component, represented by albite that exsolves from K-feldspar and is redistributed at the crystal margins. Similarly, oligoclase maintenance is formed; however, unlike the previous one, it involves high-temperature magmatic processes. The author relates these textures to the subsolvus rebalancing of alkali feldspar and the high concentrations of fluorine in rapakivi magmas.

Most of the rapakivi granites known until now is of Proterozoic age, in a range that goes from 1.0 to 1.8 Ga. However, there are bodies of rapakivi granites from the Archean and Phanerozoic eras. According to [31], rapakivi granites are A-type granites characterized by the presence, at least in the larger batholiths, of varieties of granite with rapakivi texture. They are ferroan, alkali-calcium to alkaline granites, predominantly metaluminous, sometimes peraluminous, typically mined in Sn and associated metals. The magmatic association of the rapakivi granites is bimodal (mafic-felsic); basic rocks such as diabase, gabbro, and anorthosite can be associated with rhyolites, granites, and syenites. A possible interaction between these two types of magmas can generate albite locally, and intermediate rocks [31]. The relationship between rapakivi magmatism and orogenic processes has been discussed in several studies (e.g., [12,27]). The proposed models can be classified into three main groups: (i) mafic underplating that includes at least partial melting of the crust by mafic magma of mantle origin; (ii) melting process of already thinned crust in extensional environments; and (iii) intracratonic magmatism related to orogenic processes taking place on the cratonic margins.

Although the geochemical and isotopic characteristics of rapakivi granites can be better explained based on the mafic underplating model, in which the crust melts remain unanswered. The formation of oval-shaped alkali feldspar mega crystals is most likely related to changes in the physicochemical conditions of the generation environment, which ultimately stabilizes plagioclase. It allows this mineral to border the alkali feldspar megacrysts. In general, it can be concluded that the A-type character of rapakivi granites reflects both the tectonic environment of formation and the origin of the related magmas. In contrast, the rapakivi texture reflects only the conditions of magma crystallization. Another aspect of being considered is the importance of metallogenetic, petrological and isotopic studies [32–38], which are the focus of this investigation.

3. Geological Context of the Study Area

The Amazon Craton

The Amazon Craton (Figure 1) is one of the main Precambrian geotectonic entities in South America and outcrops mainly in Brazilian territory, extending towards Bolivia, Colombia, Guyana, Paraguay, Suriname, and Venezuela. The Phanerozoic basins of Maranhão cover it to the northeast; Amazonas in the central part; Xingu-Alto Tapajós to the south; Parecis to the southeast and Solimões to the west. It is limited in the eastern portion by the Andean Orogenic belt, and in the eastern and southeastern parts by the Neoproterozoic Araguaia folded belt [39–41].

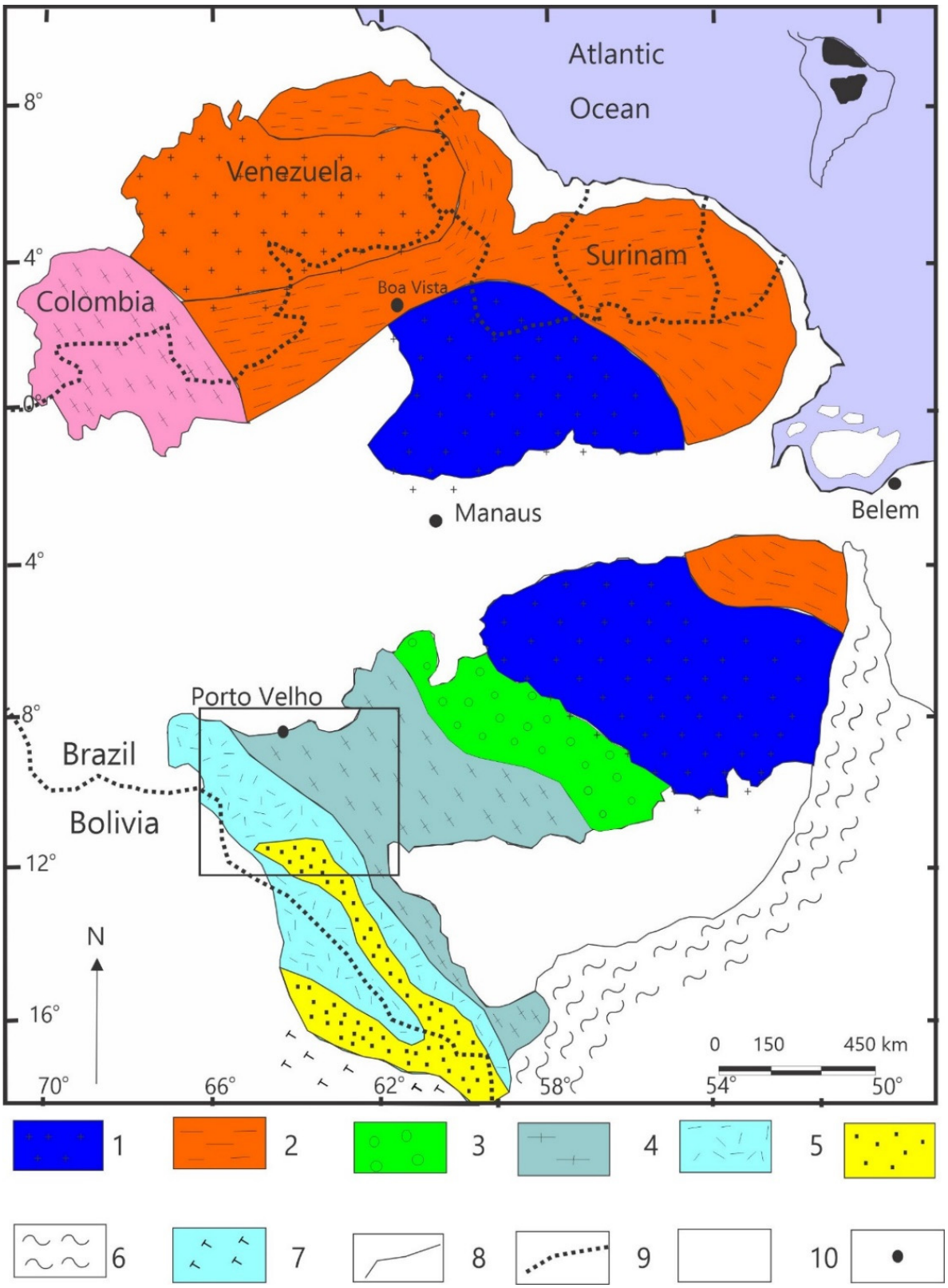

Figure 1. Subdivisions of geochronological provinces of the Amazon Craton, black rectangle indicates the location of the Rondônia Tin Province. Source: Modified from [31] with updated geochronological data according to [39–41].

Ref. [40] made the first subdivision of the craton, which consisted of the following structural provinces: (i) Rio Branco Province, belonging to the Guiana Shield to the north, and; (ii) Tapajós Province to the south, located in the portion of the Central Brazil Shield or Craton of the Guaporé. Ref. [40] divided the Craton into four geochronological-structural provinces, with the Central Amazon Province (>2.5 Ga) interpreted as the oldest nucleus and the other provinces: Maroni-Itacaúnas (2.2–1.8 Ga), Rio Negro-Juruena (1.75–1.4 Ga) and Rondoniano (1.4–1.1 Ga) as mobile belts, each with a distinct geodynamic development. Subsequent radiometric studies (Rb/Sr), reported by [41–45], were essential for the subdivision of the Craton into five or six provinces, respectively. In this sense, Ref. [45] defined the following subdivisions for the Amazon Craton: Central Amazon Province (2.3 Ga); Maroni–Itacaúnas Province (2.2–2.95 Ga); Ventuari–Tapajós Province (2.95–1.8 Ga); Rio Negro–Juruena Province (1.8–1.55 Ga); Rondoniano-San Ignacio Province (1.55–1.3 Ga) and Sunsás Province (1.25–1.0 Ga) (Figure 1).

More recent interpretations by [39] based on U-Pb geochronological data on zircons, in addition to Rb-Sr and Sm-Nd isotopic data, suggested a division of the Craton into eight geotectonic provinces. As a result, the following changes were proposed: Creation of the Carajás Province through the dismemberment of the Central Amazon Province; division of the Rio Negro—Juruena Province into Rio Negro and Rondônia-Juruena; expansion of the land of the Sunsás Province, which is now includes part of the of Rondoniano-San Ignacio Province; change of the name of the Ventuari-Tapajós Province to Tapajós-Parima and integration of part of Ventuari region (Venezuela) to the Rio Negro Province and creation of the Transamazonian Province to replace the Maroni-Itacaúmas Province. Figure 1 shows the craton compartmentation according to [43].

The State of Rondônia is inserted in the geological and geotectonic context of the SW region of the Amazon Craton, in the conception of [46–48], represented by the geochronological provinces Rio Negro-Juruena (1.80–1.55 Ga), Rondoniano-San Ignacio (1.50–1.30 Ga) and Sunsás (1.25–1.0 Ga). According to these authors, at least two magnetic arc systems marked by granitic and deformational activities between 1.8 and 1.7 Ga have been recorded in the Rio Negro-Juruena province.

Felsic volcanism and sedimentation were recorded between 1.7 and 1.65 Ga, and rapakivi granite intrusions between 1.6 and 1.51 Ga. The later system was characterized by deformation and recrystallization of syn- to late-tectonic granites, including the rapakivi granites from 1.6 to 1.51 Ga (Serra da Providência Suite), in addition to felsic volcanism and sedimentation between 1.5 and 1.4 Ga. Between 1.5 and 1.35 Ga, there is a period of stability in the Rio Negro-Juruena Province, characterized by a distensional tectonic regime with the generation of mega fractures that allowed the accommodation of the anorogenic granitic suites of Santo Antônio, Teotônio, and Alto Candeias, in addition to basic and ultrabasic rocks, sedimentation of continental rifts [49–59].

4. Rondônia Tin Province

The discovery of cassiterite in Rondônia in the 1960s stimulated the first research in the region and the characterization of features of mineralized granites [16,17]. Fluorine enrichment, association with rhyolitic volcanic rocks and breccia zones, composing a vulcanic-plutonic system were analyzed. The fact that rocks exhibit feldspars in oval shapes and concentric ring structures, aligned according to the general direction NNE-SSW [16], led to the comparison of the Rondônia tin granitic complexes with the Mesozoic Younger Granites that occur in northern Nigeria and Niger [17]. These aspects inspired the designation Younger Granites de Rondônia [17].

Rondônia Tin Province is inserted in the context of the Jamari Terrain, as shown partially in the tectonostratigraphic map (Figure 2) compiled by [18]. The first isotopic analyzes in the staniferous granitic complexes of Rondônia used the Rb-Sr method in whole rock and K-Ar in biotite and presented ages around 940 ± 20 Ma interpreted as ages of intrusion of these granitic bodies. Rb-Sr and K-Ar ages of 977 ± 20 Ma, 919 ± 20 Ma, and 1192 ± 39 Ma were reported by [19].

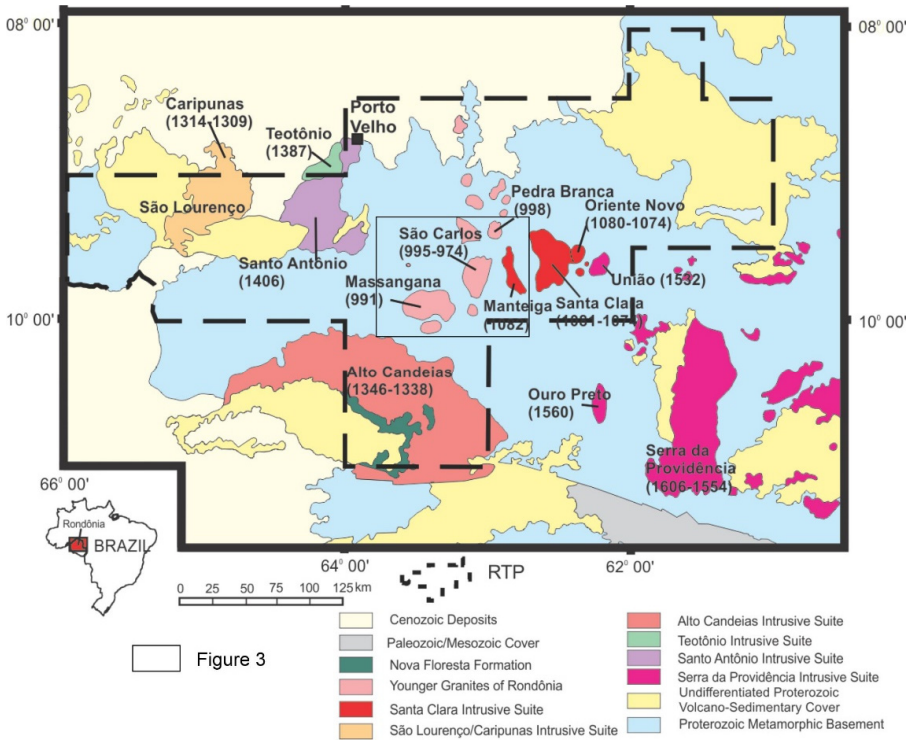

Figure 2. Limits of the Rondônia Tin Province were modified from [18,19]. The location of Figure 3 is presented as a black rectangle.

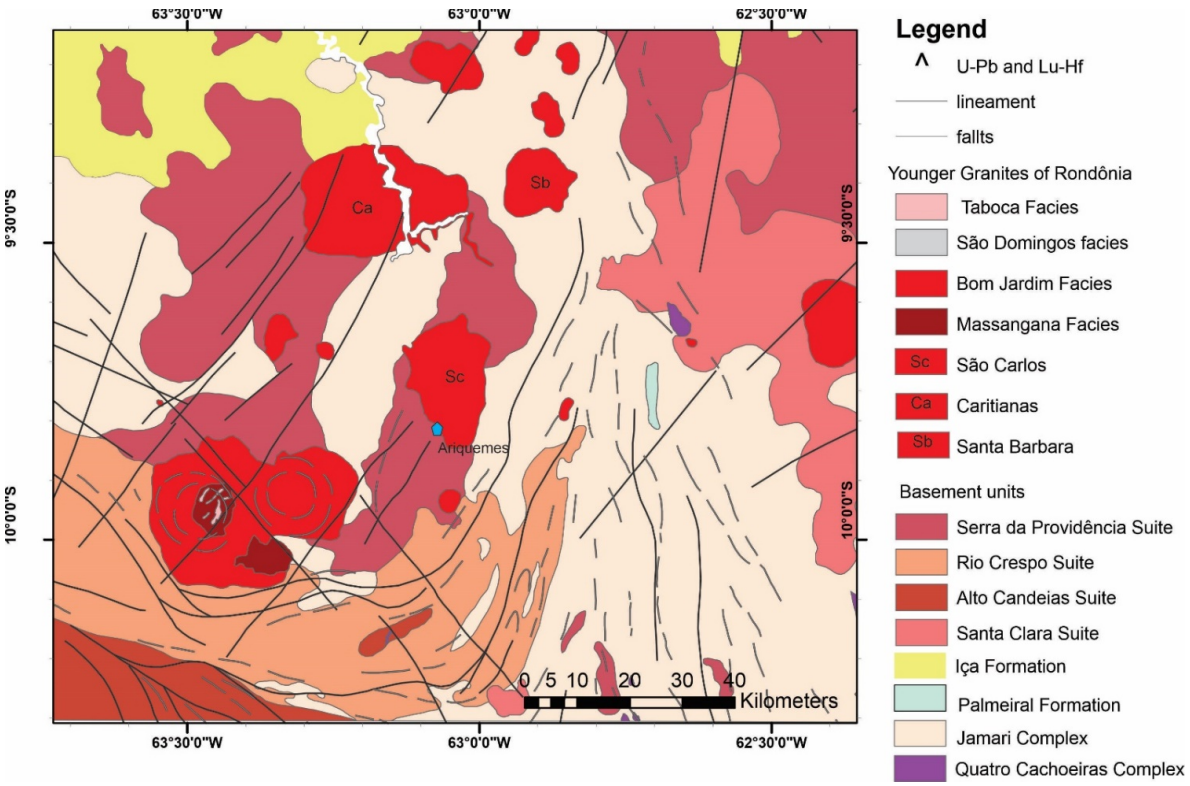

Figure 3. Schematic map with the location of all the massifs that comprise the Santa Clara Intrusive Suite; modified from [41]. Details of the Rondônia Tin Province highlighting only the intrusive suites that present tin mineralization: Alto Candeias Intrusive Suite, São Lourenço-Caripunas Intrusive Suite, Santa Clara Intrusive Suite, and Rondônia Suite.

Ref. [19] subdivided the Rondônia Tin Province into three groups: (a) Serra da Providência Suite with an abundance of rapakivi rocks (1400 to 1200 Ma); (b) Rapakivi granites and similar types younger than above (1270 to 1180 Ma); and (c) Younger Granites or Younger Granites of Rondônia mineralized in the tin (980 Ma). Ref. [47] identified four magmatic events in the Rondônia region: (a) the first event between 1545 and 1300 Ma, corresponding to the genesis of the basement granite; and (b) three other successive events, around 1270, 1025, and 955 Ma, corresponding to the anorogenic phases of the granites tin-bearing mineralizations.

The application of U-Pb, Sm-Nd, and Ar-Ar methods in geochronological investigations in the late 1990s, together with petrogenetic information, led to a new reinterpretation of the granite genesis picture in the Rondônia region. Refs. [47–50] proposed three tectonic cycles with seven subsequent episodes of rapakivi magmatism associated with mafic-ultramafic and acidic to intermediate volcanic rocks. That cycles occurred from 1600 to 950 Ma and defined the limits of the Rondônia Tin Province (Figure 2).

According to Refs. [27,46], the first cycle corresponds to the intrusion of the Serra da Providência Intrusive Suite (1606 ± 24 to 1532 ± 4.5 Ma) related to an extensional regime of the end of the Rio Negro-Juruena orogeny. The second cycle involves new magmatism that affected the Rio Negro-Juruena Province and part of the Rondoniano-San Ignácio Province corresponding to the Santo Antônio (1406 ± 32 Ma), Teotônio (1387 ± 16 Ma), Alto Candeias (1347 ± 4.7 to 1346 ± 4.6 Ma) and São Lourenço-Caripunas (1314 ± 13 to 1309 ± 24 Ma) suites. The first three suites were probably formed during a back-arc intracontinental rifting cycle that occurred in the Rondoniano-San Ignácio orogeny. In contrast, the São Lourenço-Caripunas Intrusive Suite was created during the final extensional process, before the Sunsás/Aguapei orogeny (1.25–1.00 G.a). In the third and last cycle, the Santa Clara Intrusive Suite (from 1082 ± 4.9 Ma to 1080 ± 27 Ma) and the Rondônia Young Granites (from 998 ± 0.5 Ma to 991 ± 14 Ma) were formed, considered distal representatives of the effects of the Sunsas-Aguapeí orogeny [51]. The most expressive tin deposits are associated with granitic complexes in the last magmatic phases. The Massangana, Palanqueta, São Carlos, Caritianas, Pedra Branca and Santa Bárbara massifs are part of the Rondônia Intrusive Suite (Figure 3).

The granites of the Rondônia Intrusive Suite are characterized by batholiths and multiphase and epizonal stocks, with dimensions reaching 25 km in diameter and N-S and NE-SW directions, hosted in rocks of the Jamari Complex [47]. Contacts with the host rocks are abrupt and irregular, with the sporadic presence of xenoliths (from the host). Some bodies still observe volcanic and sub-volcanic structures such as ring dykes and caldera subsidence. Chemically, the granitoid have a metaluminous to peraluminous character and are classified as A-Type granites [27].

5. Methodology

Twenty-five thin sections were prepared from the Massangana Massif and thirteen from the Serra da Providência Suite, totaling forty-three thin sheets. The petrographic descriptions were made at the Petrography Laboratory from the Universidade do Estado do Rio de Janeiro (UERJ). The thin sections were described with a Zeiss Axioskop 40 binocular microscope, with a 2.5–50 magnification lens.

5.1. U-Pb Geochronology

The LA-ICP-MS combines the inductively coupled plasma mass spectrometry (ICP-MS) technique with a laser ablation (LA) system. This technique involves volatilization of the sample by a laser beam followed by ionization by an induced plasma (ICP) that allows the analysis of grains or parts of individual grains [60]. The possibility to perform punctual analyses and the quickness with which these are performed are the advantages of this method, especially for zircon grains, which can have different ages at the edge and in the core. Another advantage of this method is the low susceptibility to contamination, unlike the isotopic dilution technique. The equipment used in the U-Pb and Lu-Hf analysis

of this investigation was a Neptune Plus with seven electron multiplier and nine faraday collectors. The equipment is coupled to an Excimer Laser Photon Machines 193 mm with a He gas flow of 0.750 L/min. For the U-Pb analyses, a repetition rate of 7–9 Hz was used. For the Lu-Hf analysis, a repetition rate of 10 Hz was required. The diameter of the laser craters was 30 μ for U-Pb analysis and 40 μ for Lu-Hf.

Four representative samples of the different types of rocks from the Massangana intrusion were selected for the U-Pb and Lu-Hf isotopic analyses. In the initial processing, approximately 20 kg of each sample chosen were washed, crushed, and pulverized in standard equipment and under strict cleaning criteria. The minerals were concentrated in bromoform to separate light grains. After separating the heavy fraction, these minerals were submitted to an electromagnetic separator (FRANTZ) under different degrees of inclination. After this process, the zircon grains present in the fractions were collected in a binocular magnifying microscope based on morphological criteria. All zircons were mounted on a 2.5 cm diameter circular section of Araldite and polished until the zircons were exposed. The grains were imaged using a scanning electron microscope (FEI—QUANTA 250) to obtain images by cathode-luminescence.

5.2. The Lu-Hf Method

The $^{176}Hf/^{177}Hf$ ratio in zircon may be the initial value during crystallization [61]. In addition, the high resistance of this mineral to later thermal events makes the U-Pb and Lu-Hf methods in zircon even more interesting. The chemical properties of Lu-Hf are similar to those of the Sm-Nd during the partial mantle melting process. Similarly, as Nd isotopes, the Hf isotopic values can be expressed as $\varepsilon_{Hf.}$ which consists of comparing the $^{176}Hf/^{177}Hf$ ratio of the studied sample at the time of its formation with those of the uniform chondritic reservoir (CHUR) default. A positive value of ε_{Hf} means that the parent magma has a higher ratio than the chondrite; therefore, the source is the mantle. A negative ε_{Hf} value implies that the magma that formed this rock had a lower $^{177}Hf/^{176}Hf$ ratio than the chondrite; therefore, it is related to a crustal origin. The higher the value of positive ε_{Hf}, the more geochemically depleted in Hf is this mantle from which the material was derived. Another important datum provided by the Lu-Hf system is the model age of the depleted mantle, or T_{DM} (Depleted Mantle) age, which is calculated from the initial Hf isotopic composition at the time the zircon crystallized and the Lu/Hf ratio of the precursor crust [45]. The T_{DM} age indicates the crustal residence time of the zircon host rock. Current values assumed for the depleted mantle are 0.28325 for the $^{176}Hf/^{177}Hf$ ratio and 0.0388 for the $^{176}Lu/^{177}Hf$ ratio [61].

6. Results

The Massangana Massif is a considerable intrusion (about 900 km^2 of surface; Figure 4) and outcrops mainly in the form of extensive slabs, blocks, and boulders embedded in rocks of the Jamari Complex and the Serra da Providência Suite. Through satellite images and geophysical surveys [58], two circular intrusions in the Massangana Massif were mapped, consisting of coarse-grained rocks with perthitic microcline as a phenocryst. In the central part of the intrusion, circular intrusions are composed of medium to coarse-grained biotite granites, surrounded by hornblende-microcline granites. The southeastern portion of the Massangana Massif records the São Domingos intrusion, characterized by at least three distinct types of biotite-granite. Tin mineralizations occur near the boundaries between the two lithotypes.

The lithofacies were separated mainly according to the variation of the mafic and felsic mineral present; aspects such as grain and texture were also considered. Thus, four main lithofacies are recognized: (1) Massangana Facies with variations from biotite-granite, hornblende granite, and piterlite; (2): Bom Jardim Facies with components such as biotite-granite and biotite alkali granite; (3) Taboca Facies represented by albite granite. In the south/southeast portion of Massangana Facies, there is a granitic pluton almost disconnected from the rest of the massif, making only contact at the SE edge through abrupt

and irregular contact with the host [47]. This granite stock is called the São Domingos Massif, where the compositions of albite granite and alkali granite can be observed. This area, along with the central-west portion (a region called Taboca), presents the exposures of primary mineralizations gathered as Massangana, where the exploration of secondary deposits (placer) from this region has been concentrated since the 1950s.

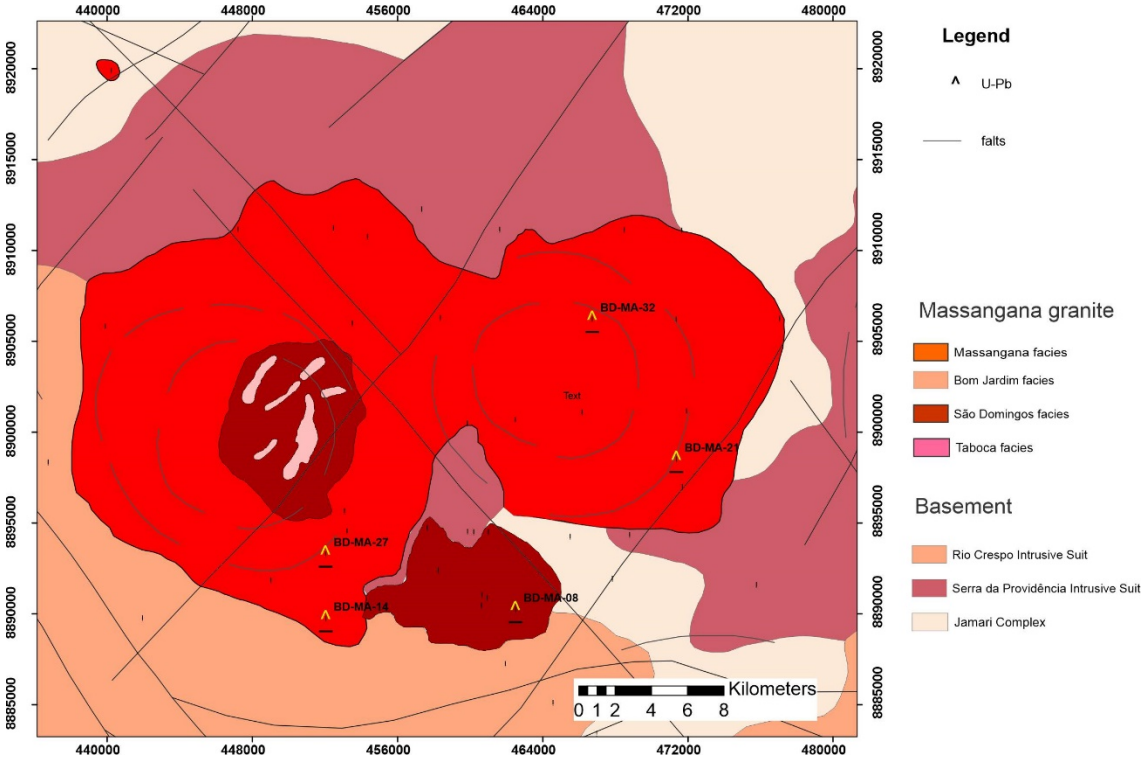

Figure 4. Geological map of the Massangana Massif showing sampled points.

Massangana Granite Lithofacies

Fieldwork and petrography indicate three main lithofacies: (1): biotite-granite, (2): biotite-hornblende-granite, (3) fine to medium biotite-granite. Ref. [59] also indicates two other facies, called Bom Jardim, totaling four facies characterized below.

(A) Massangana Facies

The Massangana magmatic facies represents about 80% of the massif with porphyroid to pegmatite or coarse-grained granites, with microcline and eventually orthoclase as the primary phase. The predominant lithotypes of Massangana Facies (in unmineralized zones) are coarse to very coarse-grained granites that have biotite as the main. Still, usually the only mafic mineral, as well as microcline, and orthoclase, coexisting as the main felsic minerals. They frequently outcrop in the northern, northeastern, and southeastern portions of the granitic pluton with marginal variations for pyterlite types, these in the form of pockets in the medium-grained porphyritic granites.

(B) Biotite Hornblende Granite

In the eastern portion (Figure 4), there is a concentration of biotite-granites and biotite-hornblende, coarse to very coarse-grained granites, sometimes porphyritic with rapakivi texture. In contrast, the SW portion is composed of medium to coarse-grained biotite-granites intruded by fine-grained granites and pegmatites in the form of dikes and pockets.

The agglomerates of mafic minerals are common among coarse grains (Figure 5A), changing laterally to medium-grained granite. Quartz grains are generally anhedral and occur in contact with feldspar crystals, interstitial clusters, or large crystals (>1 cm in diameter) with irregular edges. Orthoclase is the primary feldspar in most samples, occasionally replaced by microcline. Orthoclase occurs in the form of large crystals (>1 cm in diameter)

anhedral to subhedral with a perthite to mesoperthite texture. The microcline has a subhedral shape; its size varies between 0.5 and 1.0 mm, in addition to a perthite and tartan texture. Plagioclase is usually interstitial and occurs in the form of small tabular slats.

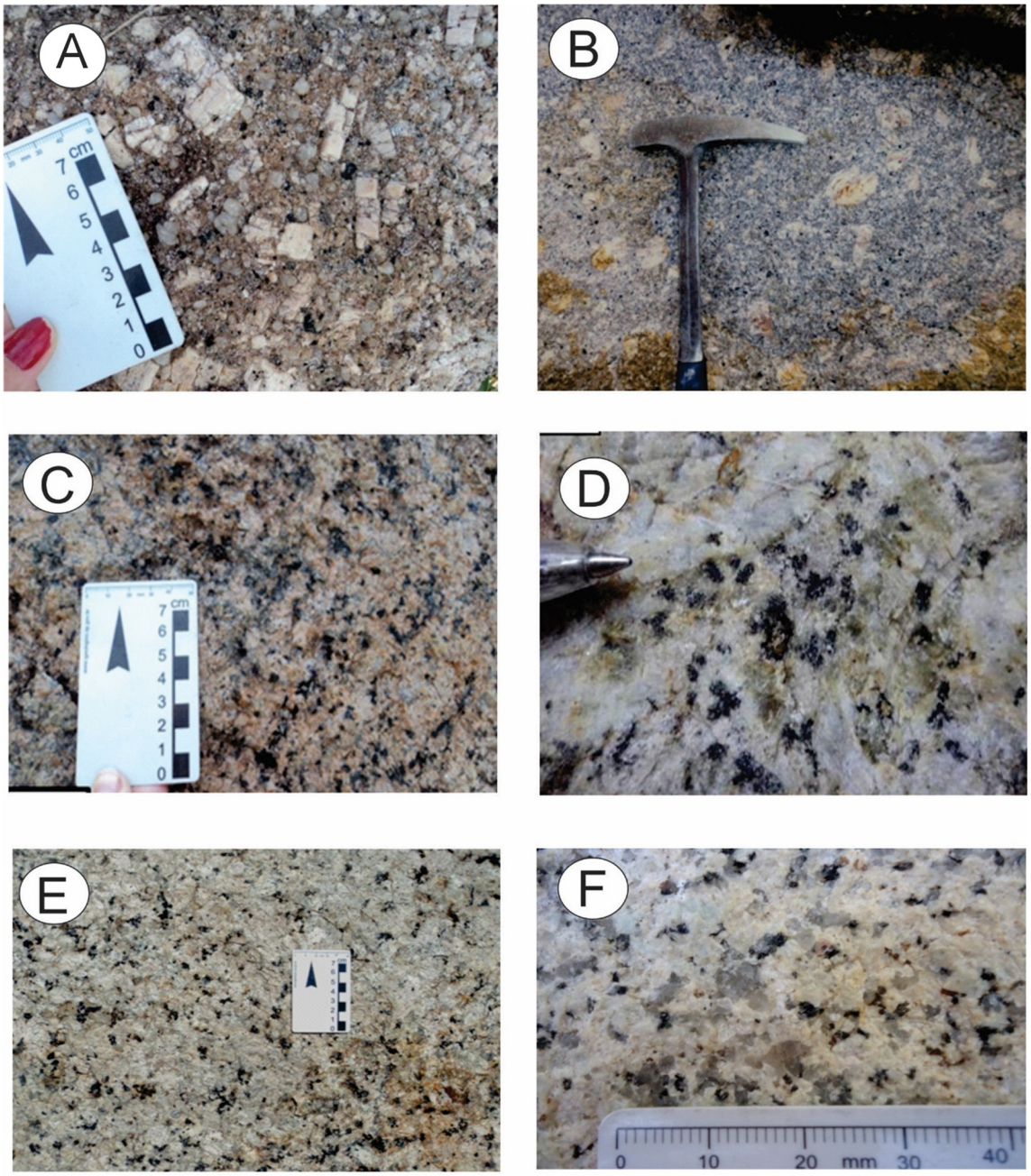

Figure 5. Outcrops and macroscopic features of the Massangana intrusion. (**A**) Massangana Facies biotite-hornblende is coarse to porphyritic granite. (**B**) Massangana facies medium gray to pinkish matrix pyterlite with tabular K-feldspar phenocrysts and rounded phenocrysts; (**C**) Bom Jardim porphyritic biotite granite with rapakivi texture showing intergranular arrangement between K-feldspar, quartz, biotite, and plagioclase, as well as accessories, allanite, zircon, and fluorite. (**D**) Bom Jardim Facies outcrop in the form of medium biotite syenogranite; (**E**) Taboca facies albite granite isotropic texture; (**F**) São Domingos Facies alkali granite with coarse texture with two generations of quartz.

Biotite is the only mafic mineral present in most of the observed samples, presenting a brown or reddish color, and occurs as well-formed lamellae, sometimes with irregular

edges (Figure 6A). In some instances, it is scarce and presents a reddish color with serrated edges and features of hydrothermal alteration. The presence of pleochroic halos is frequent in biotite, mainly due to the inclusion of zircon and allanite crystals. The amphibole, when present, displays a euhedral (rare) to subhedral (familiar) shape and dark green color, evidencing high Fe content. The association of hornblende with biotite usually occurs through interdigitated contacts, which evidences the crystallization of biotite at the expense of hornblende or a simultaneous crystallization of these two minerals. Some samples show only hornblende as mafic minerals; in this case, it is pale green, making it challenging to observe the cleavage.

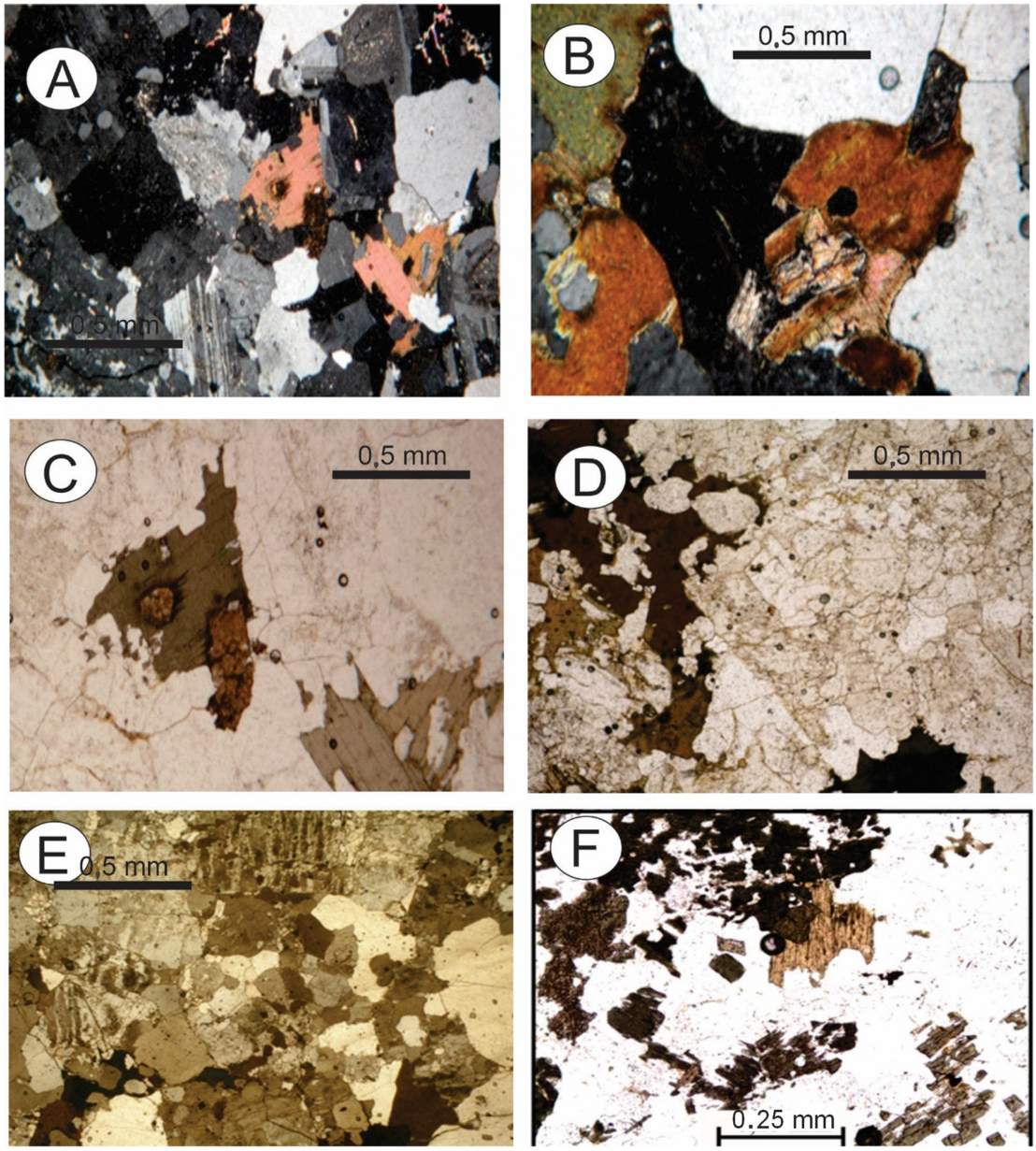

Figure 6. Microscopic features of Massangana intrusion; (**A**) Massangana porphyritic facies, showing matrix, composed of quartz and anhedral feldspar, the latter with sericitic alteration and hornblende; (**B**) Pyterlite porphyritic showing hornblende and oval K-feldspar phenocrysts and medium matrix. In (**C**) Bom Jardim Facies showing perthitic K-feldspar phenocryst in contact with biotite lamella and matrix; (**D**) detail with parallel nicols hornblende green crystals, intergrown with biotite; (**E**) Taboca Facies with sericitization of plagioclase; (**F**) São Domingos medium gray to pinkish medium matrix granite with tabular K-feldspar phenocrysts with potassium alteration.

(C) Pyterlite

An important area in the Massangana Facies is represented by porphyritic granites (subrounded feldspars) here called pyterlites. Porphyritic granites were collected in the southwestern and north-central portions of the Facies Massangana. Porphyritic granites are classified as pyterlites because most phenocrysts are oval (Figure 5B) with rare oligoclase-andesine-mantled K-feldspar crystals, in addition to hornblende and biotite (Figure 6B). Pyterlite occurs in the form of extensive outcrops, generally close to coarse to very coarse granite, and due to petrographic similarities, it is grouped in the biotite-hornblende-granite facies on the geological map. Accessory minerals are composed of zircon, fluorite, and allanite.

Bom Jardim Facies

The Bom Jardim Facies constitutes an ellipsoidal stock with irregular contours and a diameter of about 10 km, intruded into the Massangana Massif through abrupt and interpenetrative contacts, with many enclaves. It presents excellent textural variation, from micro granular to porphyritic granites and microgranite dykes, mainly in the central part of the stock. The two variations have a color ranging from beige to whitish and a matrix composed of anhedral quartz crystals, plagioclase in the form of small slats, biotite, and hornblende. Phenocrystals are generally tabular to oval, represented by orthoclase, as described below:

(A) Biotite granite

The studied rocks have an equigranular texture (Figure 5C) with the main mineralogy composed of orthoclase (50%), always with perthites, quartz (20%), sometimes forming a triple junction, showing a recrystallization process, plagioclase (20%) in short interstitial slats and mafic minerals represented by beige (6%) to brown biotite and hornblende (5%) (Figure 6C). K-feldspar may show sericitization. Accessories are fluorite, zircon, and allanite.

(B) Biotite alkali granite

In the Southwest portion (Figure 4), medium-grained types that frequently exhibit K-feldspar phenocrysts slightly larger than the average matrix are more common (Figure 5D). Rocks of two compositions were identified; the first was composed of biotite-amphibole-granite, and the second was composed of biotite-granite. K-feldspar presents sizes and is frequently sericitized. Biotite with pleochroism ranging from beige to reddish.

The most frequent accessory minerals are zircon in the form of short, generally fractured prisms; titanite, with beige color and euhedral-angular habit or in cross-section with the rhombohedral pattern (Figure 6D). Opaque minerals, usually anhedral, often occur near or included in the biotite, as well as epidote, topaz, fluorite, allanite, and apatite. Secondary mineralogy is represented by sericite, which mainly affects plagioclase and can be pervasive throughout the blade, in addition to chlorite, as an alteration product of biotite, muscovite in a smaller proportion, and Fe and Ti oxides.

Taboca Facies

Syenite rocks characterize the Facies Taboca (Figure 4), intruded in the Bom Jardim and São Domingos Facies. For São Domingos Facies, the field relationships were inconclusive, so [48] geological map was used to draw the boundaries. Petrographic variations include mainly syenite, quartz-syenites, and quartz-monzonites.

The biotite-syenogranite facies has a fine to medium equigranular texture (Figure 5E) composed of microcline, quartz, plagioclase, and biotite. The microcline occurs in the form of tabular to anhedral subhedral crystals with characteristic tartan twins, in addition to simple twinning, in some crystals and sizes up to 1 mm in length. Quartz occurs in the form of anhedral grains about 0.1 mm in diameter. Plagioclase usually occurs in the form of tabular subhedral crystals, with irregular edges and sizes ranging from 0.1 to 0.5 mm in length, presenting polysynthetic twinning following the albite law and simple twinning. More restrictedly, crystals of anhedral plagioclase also occur, some with intense sericitization, which is concentrated in the center of the crystal, forming a sericitic core,

with the edges changing to another feldspar, possibly the microcline, in contact with this crystal (Figure 6E).

Bbiotite occurs in two ways: one is short, isolated lamellae, beige to reddish or greenish in color, with intense alteration and percolation of orange-colored oxidizing fluid; the other, in clusters with pleochroism ranging from light beige to brown. These features are perhaps evidence of two generations of biotite, one primary, which occurs in the form of agglomerates (clots), and the other interstitial, which occurs in isolation between the larger crystals of feldspars and quartz. Accessory minerals are represented by zircon, titanite, and opaque minerals, usually included or in contact with biotite lamellae. Alteration minerals are represented by sericite, that occurs as an alteration product of plagioclase, muscovite, and chlorite that are concentrated at the edges and cleavages of biotite.

São Domingos Facies

São Domingos Facies occurs in contact with Massangana Facies, and field features indicate that it is an independent intrusion. In the SW portion of the massif, it is common to find microgranites of monzogranitic or alkali-granitic composition in the form of lenses, veins, or pockets, as well as intrusive pegmatitic veins and pockets of medium to coarse-grained granite. Still, they do not occur as widely as in Massangana Facies, but in a localized way. These texture variations can also occur in bands. The texture variation suggests that they are coeval (Figure 4).

(A) Albite granite

São Domingos region (southern portion of the massif) is detached from the rest of the Massangana Massif and partially in contact on the southeastern edge, where there are apophyses of the São Domingos Facies of tens of meters intruded into the Massangana Facies, notably in the existing topographic highs at the head of the river. João Soares stream, as highlighted by [48]. The region is also characterized on the northern edge by intense greisenization and, to a lesser extent, on the southeast and northeast edges, affecting both the granitoid and the enclosing rocks.

The microscopic aspects of the São Domingos Facies generally present arrangements of microcline, quartz, plagioclase, biotite (Figure 5F), and muscovite (or zinnwaldite) resulting from hydrothermal alterations. There is still monazite (Figure 6F) and a large amount of opaque and pleochroic halos in the biotite crystals due to the inclusion of zircon crystals. Petrographic details of these facies are presented in the mineralizations item since these facies are more critical in terms of mineral occurrence in the context of Massangana granite.

(B) Alkali granite

The São Domingos Facies (Figure 4) is described as a granitic stock with irregular contours, arranged semi-parallel to the regional lineation of the Jamari Complex and making minute contact with the Massangana phase, where enclaves of this are frequent, in addition to enclaves of migmatites, gneisses, and amphibolites. This unit presents complex compositional variation due to mineralization processes by co-magmatic fluids that will be described in detail in the mineralization item below.

Figure 7 presents a diagram with a proposal for the evolution of the rocks that make up the Massangana granite. In this sense, the Massangana Facies is the first to be crystallized, including its variations (coarse, medium, fine, and pyterlite granites). The Bom Jardim Facies granites were defined by [47] and their contact relationships indicate that they are younger than the Massangana Facies. The São Domingos and Taboca Facies do not present a relationship that allows the discrimination of their temporal relationships, as both present equivalent mineralization and petrographic variations and are interpreted as the final stages of the magmatic fractionation process.

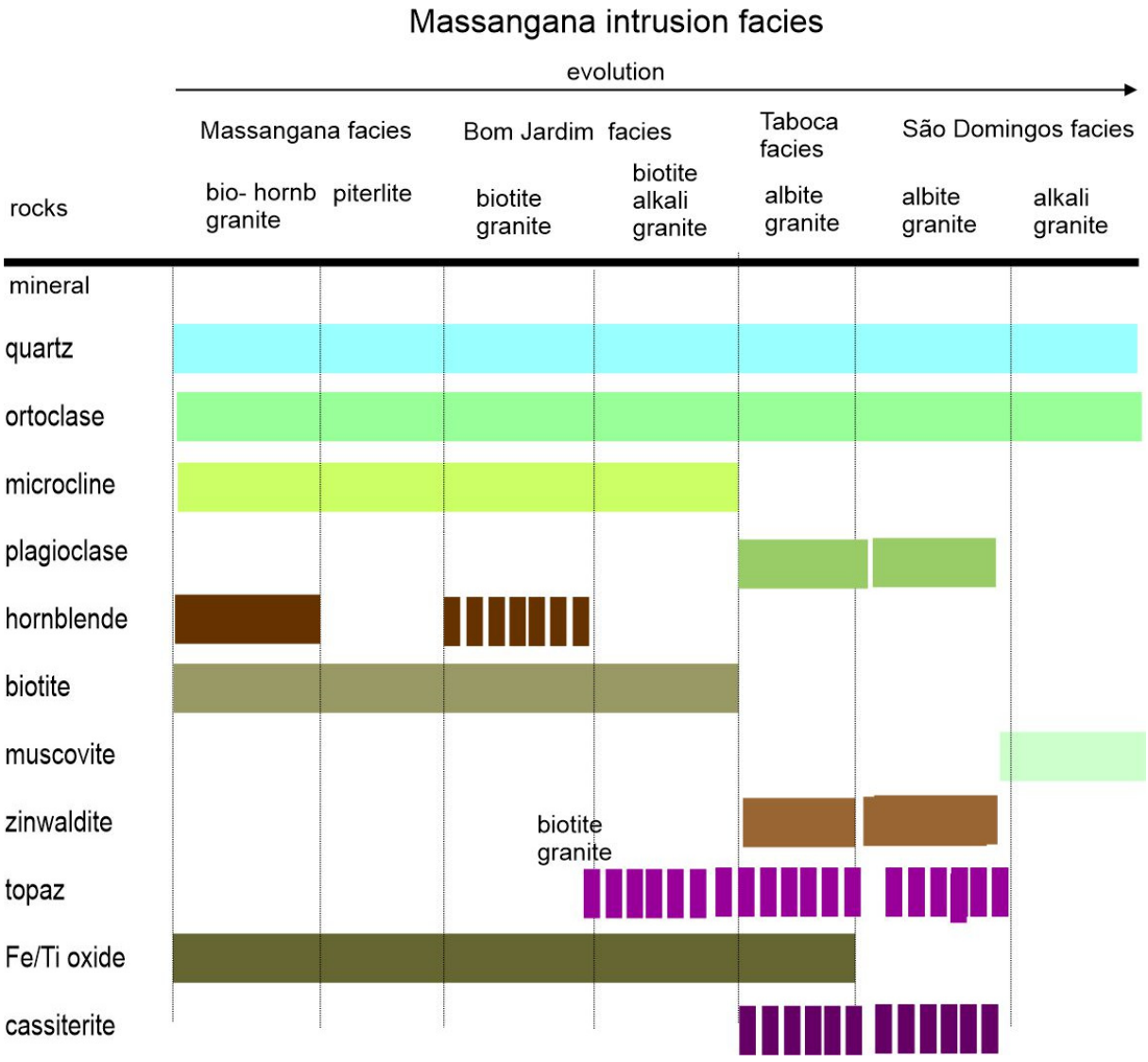

Figure 7. Evolution table of Massangana granite facies from their mineral paragenesis. The biotite and hornblende granite is interpreted as the first to be crystallized, followed by the Bom Jardim. The São Domingos and Taboca facies present equivalent mineralization and petrographic variations and are interpreted as the final stages of the magmatic fractionation process.

6.1. Characterization of Mineralized Bodies

The region of São Domingos represents the most significant production of cassiterite in the context of Massangana granite spread over several mining fronts. These exploration areas allow visualization through openings on the surface and subsurface through shafts and tunnels. The relationships between magmatic facies and mineralized bodies are complex and difficult to characterize. They will be addressed in this investigation tentatively in order to understand the evolution of magmatic fluids that resulted in mineralized bodies of economic importance. In this sense, the mineralized bodies identified here, such as endogreisens, exogreisens, pegmatites, and quartz veins, are described and analyzed.

Two types of endogreisens were observed laterally in the São Domingos area; the first formed because of the evolution of a biotite-granite that passes to albite-granite ending in greisen (and topazolite), and a second that starts from an alkali-granite evolving to medium equigranular biotite-granite climax in zinnwaldite -topaz-greisen. The two types are characterized below.

(A) Endogreisen A

The first endogreisen is interpreted as a product of the alteration of a protolith composed of biotite-granite that evolves to albite-granite and transforms into endogreisen (Figure 8A; see Figure 9A for respective tin section) with the original rocks (Figure 8B; see Figure 9B for separate tin sections) as host, a hypothesis supported by the local context where these rocks are identified with contact relationships (Figure 8C; see Figure 9C for respective tin section) with progressive lateral change, ending with the endogreisen with abrupt contact with the original magmas. These contact relationships suggest the evolutionary sequences proposed here, justified by the illustrations throughout the text. Thus, the rocks (biotite-granite and albite-granite) are interpreted as evolutionary precursors. The final products of metallogenetic evolution composed of endogreisens of different compositions will be presented. The sequence of presentation of the greisens also indicates an evolution hypothesis for the components of the studied ore.

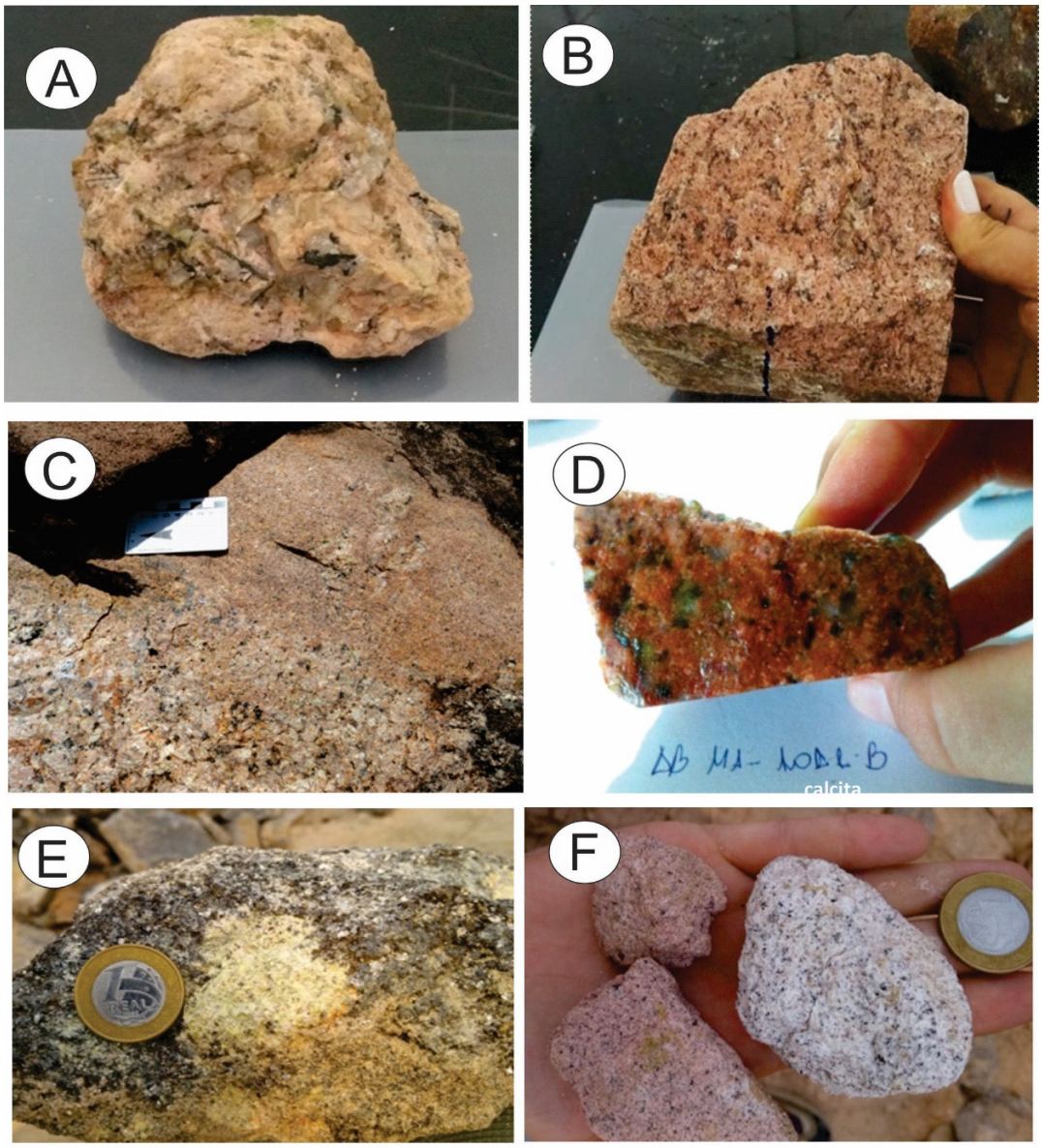

Figure 8. Macroscopic samples of endogreisens A. (**A**) Endogreisens with coarse texture K-feldspar and quartz-rich; (**B**) Intergranular arrangement of less evolved facies granite showing microcline and euhedral plagioclase; (**C**) Greisen sample with porphyry feldspar; (**D**) Outcrop of medium biotite-granite cut by coarse granitic greisen; (**E**) Tabular microcline crystal with perthitic texture, locally with plagioclase euhedral crystal inclusions; (**F**) Fragments of greisenized alkali granite.

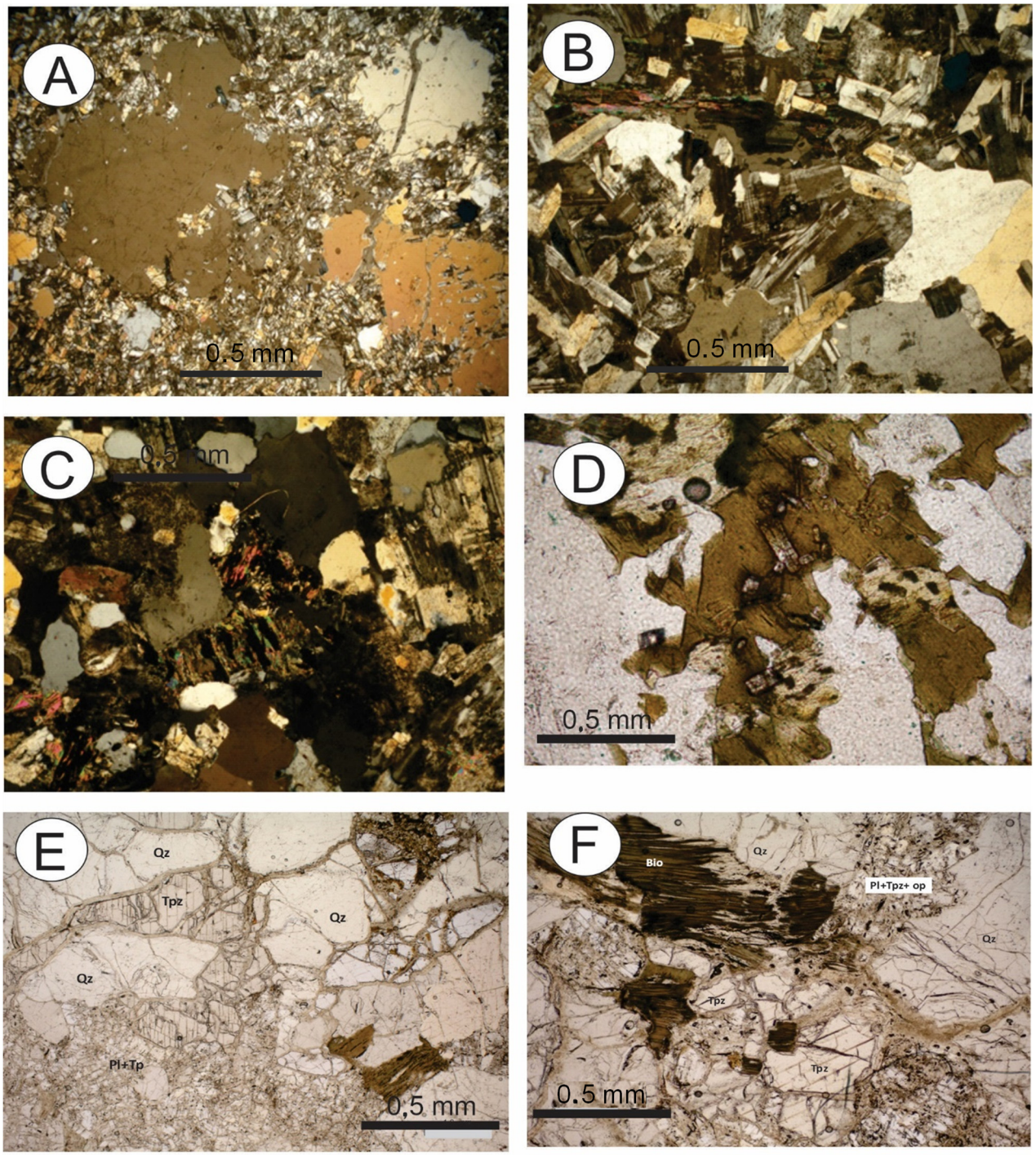

Figure 9. Macroscopic aspect of Endogreisen A characterized by mineralized medium-grained biotite-granites that make up the São Domingos Region. (**A**) medium biotite-granite with green to brown biotite grains; intensely perthitized K-feldspar, interstitial plagioclase; and (**B**) development of round quartz crystals. (**C**) Microscopic feature of fine alkali-granite with albite, quartz, and micas associated with mafic minerals; (**D**) Albite-granite with larger quartz crystals and lath-shaped subhedral plagioclase crystals, with a characteristic twin of albite changing from orthoclase to sericite; (**E**) zinnwaldite-albite granite showing opaque with zinnwaldite; (**F**) zinnwaldite grains with reaction with topaz an, quartz and plagioclase.

The mineral paragenesis presented here was obtained by petrographic analysis of samples related to endogreisen demonstrating an evolution (Figure 8D; see Figure 9D for

respective tin section) from biotite granite to topaz granite reaching topazolite (Figure 8F; see Figure 9F for separate tin section). The biotite sample also demonstrates an advanced evolutionary stage that can progress to topaz-zinnwaldite and end up in quartz-greisen.

Biotite granite

The biotite granite host rocks are the main outcropping lithofacies in the São Domingos Facies. Regionally (in terms of Massangana granite), coarse to porphyritic types are predominant locally in São Domingos Facies. The medium-grained equigranular to inequigranular types occur in the form of slabs. The medium biotite-granite that makes up most of the rocks in the central portion of the São Domingos granitic stock (in the terms used by [47] is pink in color with the primary mineralogy composed of microcline, subhedral quartz, albite, and accessory minerals; plagioclase with euhedral to subhedral crystals is usually interstitial and occurs in the form of short laths with polysynthetic albite twins. Albite and microcline crystals are commonly sericitized. K-feldspar is usually intensely perthitic and sometimes surrounded by an albite crown, forming a micro-rapakivi texture. Biotite occurs in the form of reeds with corroded edges, having pleochroic halos due to zircon inclusions. As accessories, there are fluorite, zircon, opaque, allanite, topaz, and, less frequently, muscovite. Alteration minerals are represented by sericite and chlorite.

Albite granite

This rock has its best exposure in the southern portion of the São Domingos facies, where it is opencast mining. Still, it can also occur in the form of dykes or intrusive pockets in medium to coarse biotite-granites, with gradual contacts. The greisen bodies appear to migrate from the albite granite as they present lateral variation without sharp contacts. It offers a fine to very fine-grained pink to reddish texture with primary mineralogy composed of K-feldspar (33%), quartz (35%) and/or topaz (8%–10%), plagioclase (22%) and biotite (5%–7%).

A second-hand specimen is composed of a medium-grained, pinkish-colored rock composed of lath-shaped euhedral subhedral plagioclase (albite) (65) %, ranging from 1 mm to 3 mm randomly distributed in the matrix surrounding larger quartz crystals. Microcline also occurs sparsely, and mica is very scarce <2% and occurs in an interstitial form (possibly zinnwaldite). Topaz may occur; it is difficult to differentiate it from quartz. Topaz appears to have more significant relief and fracture. Some plagioclase crystals have fractures filled with oxide and opaque minerals with reddish edges (in the reflected light, they have white dots inside). Change to sericite in some plagioclase crystals.

Zinwaldite-Albite Granite

The albite-granite sample is composed of a fine to medium-grained pink to reddish rock whose primary mineralogy is composed of lath-shaped subhedral plagioclase with serrated edges (50%), quartz (35%) and zinnwaldite (8%–10%). Lath-shaped plagioclase makes up most of the matrix in contact with larger quartz crystals. Opaque minerals in the cleavage planes commonly accompany Zinnwaldite. Orthoclase occurs as sparse spots in the albite matrix or almost wholly changed to sericite. The zinnwaldite -albite granite sample shows quartz occurring in the form of anhedral minerals with rounded edges, suggesting recrystallization. The predominant feldspar is the microcline that occurs in subhedral shapes. Biotite occurs with green to brown pleochroism, and in the portions close to the greisens zone, it is replaced by white mica (zinnwaldite). Accessory minerals are mainly represented by opaque minerals associated with micas. Alteration: chloritization of biotite and sericitization of plagioclase.

Figure 10 is the proposed evolution of the magma fractionation with initial biotite granite and topaz granite transforming into topazine and biotite ending as mica greisens: constituted almost essentially by micas that show black and silver coloration to the naked eye. A medium zinnwaldite and topaz greisen in contact gradually pass to fine alkali-granite. This dark-colored greisen features topaz and quartz as mineralogy. The micas present in quartz veins were identified as zinnwaldite and siderophyllite. It also features plagioclase and zircon as an accessory.

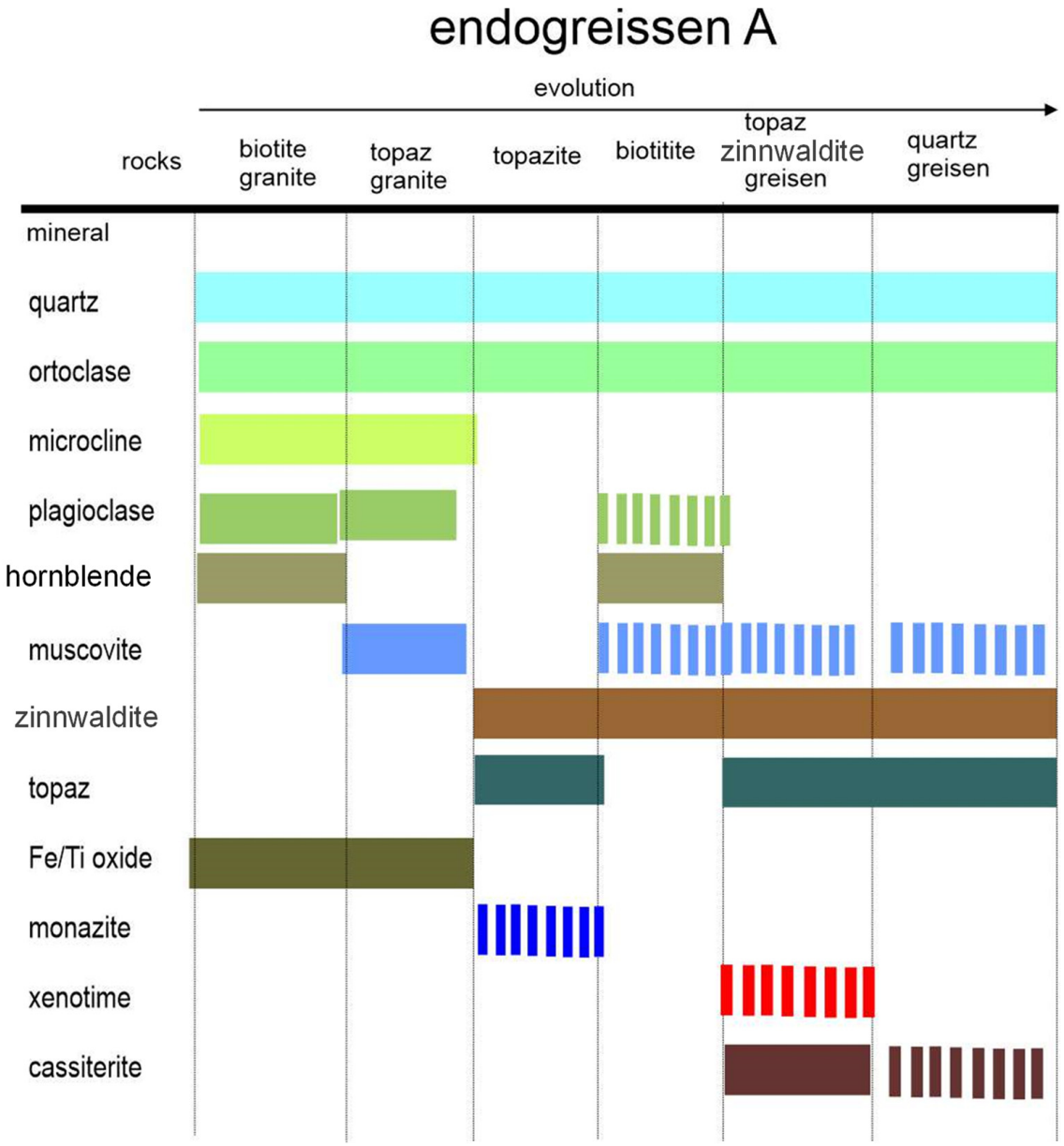

Figure 10. Mineral paragenesis was obtained by petrographic analysis of samples related to endogreisen A. The biotite-granite initial magma passes to topaz-granite ending in greisen (and topazite), ending in zinnwaldite-topaz greisen and quartz-greisen.

(B) Endogreisen B

The second type of endogreisen follows the biotite-granite evolution to alkali-granite, ending in zinnwaldite-greisen. These mineralized bodies, characterized as endogreisens B, develop in fine pink alkali-granite and medium-sized equigranular biotite granites. This contact relationship (greisen-fitting) and petrographic studies indicate that biotite-granite is the precursor in magmatic evolution, followed by alkali-granite.

Fine to medium biotite granite facies

The coarse to very coarse granite rocks were collected in an open pit mining front and are represented by greisens that always occur in contact with fine-grained granitic (Figure 11A), in the form of intrusive dykes, or as enclaves (with up to 20 cm in diameter) or even through gradual contact with the coarser-grained granite. They present fine to medium inequigranular texture, yellowish to pinkish coloration, and main mineralogy composed of microcline, quartz, plagioclase, and biotite (Figure 12A). The biotite-granite rocks present

quartz (20%–25%) with a xenomorphic habit and usually occur in an interstitial form between the larger crystals of sericitized feldspars. Some grains reach up to 0.2 mm in diameter (Figure 11B).

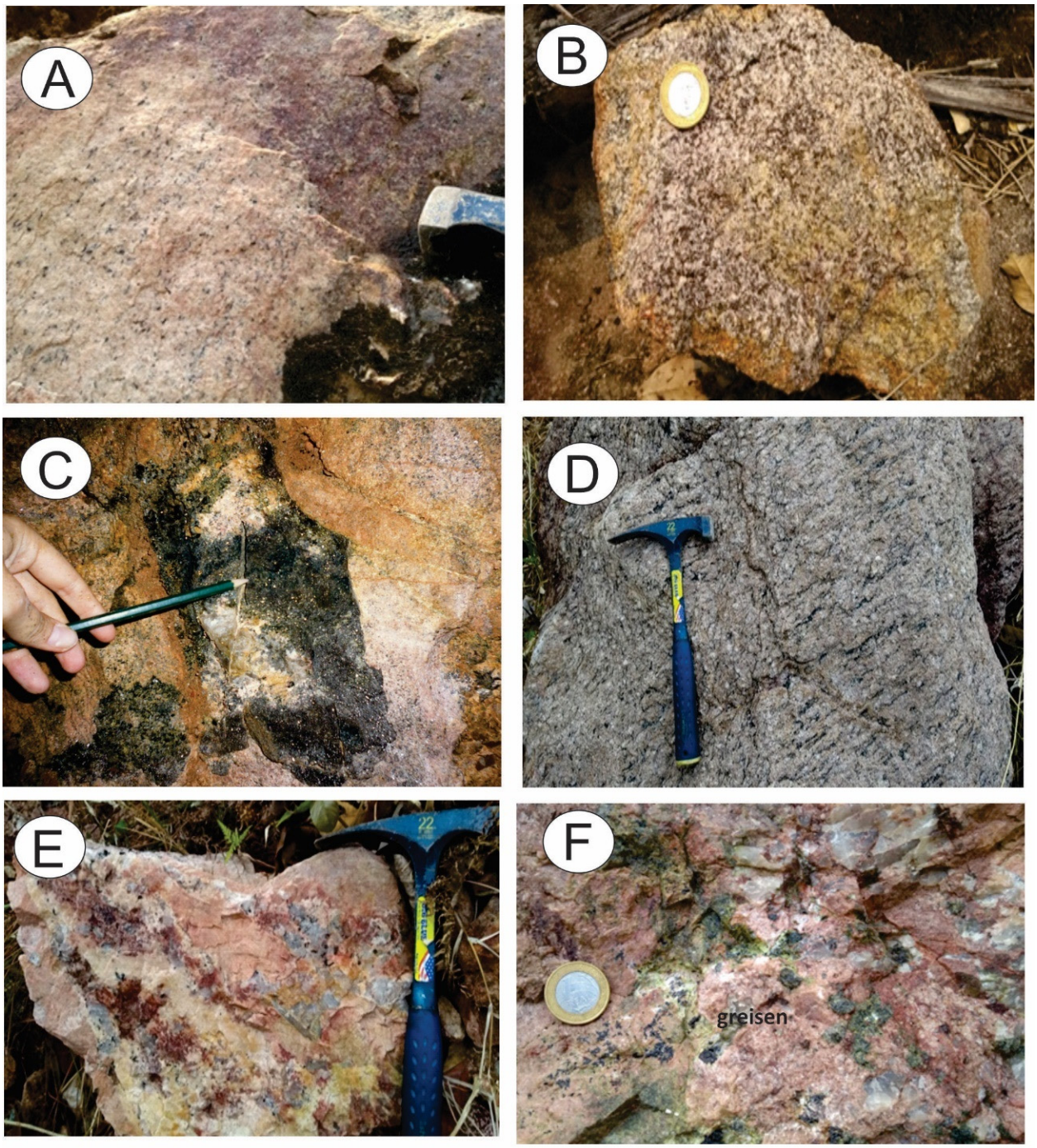

Figure 11. Endogreisen B samples and photographs of samples of the biotite-granite facies related to the endogreisens that make up the São Domingos Region. (**A**) Fine textured biotite with a medium pinkish granite in contact with fine-grained granite gradually changing to zinnwaldite-greisen; (**B**) contact of biotite-granite with topaz-alkali-granite, gradating to coarse or pegmatitic facies; (**C**) fine texture detail of alkali-granite showing sericitized K-feldspar; (**D**) Alkali-granite outcrop showing lenticular quartz veins in (**E**) contact with alkali-granite and alkali-granite topaz; (**F**) Macroscopic appearance of endogreisens associated with topaz-alkali-granite.

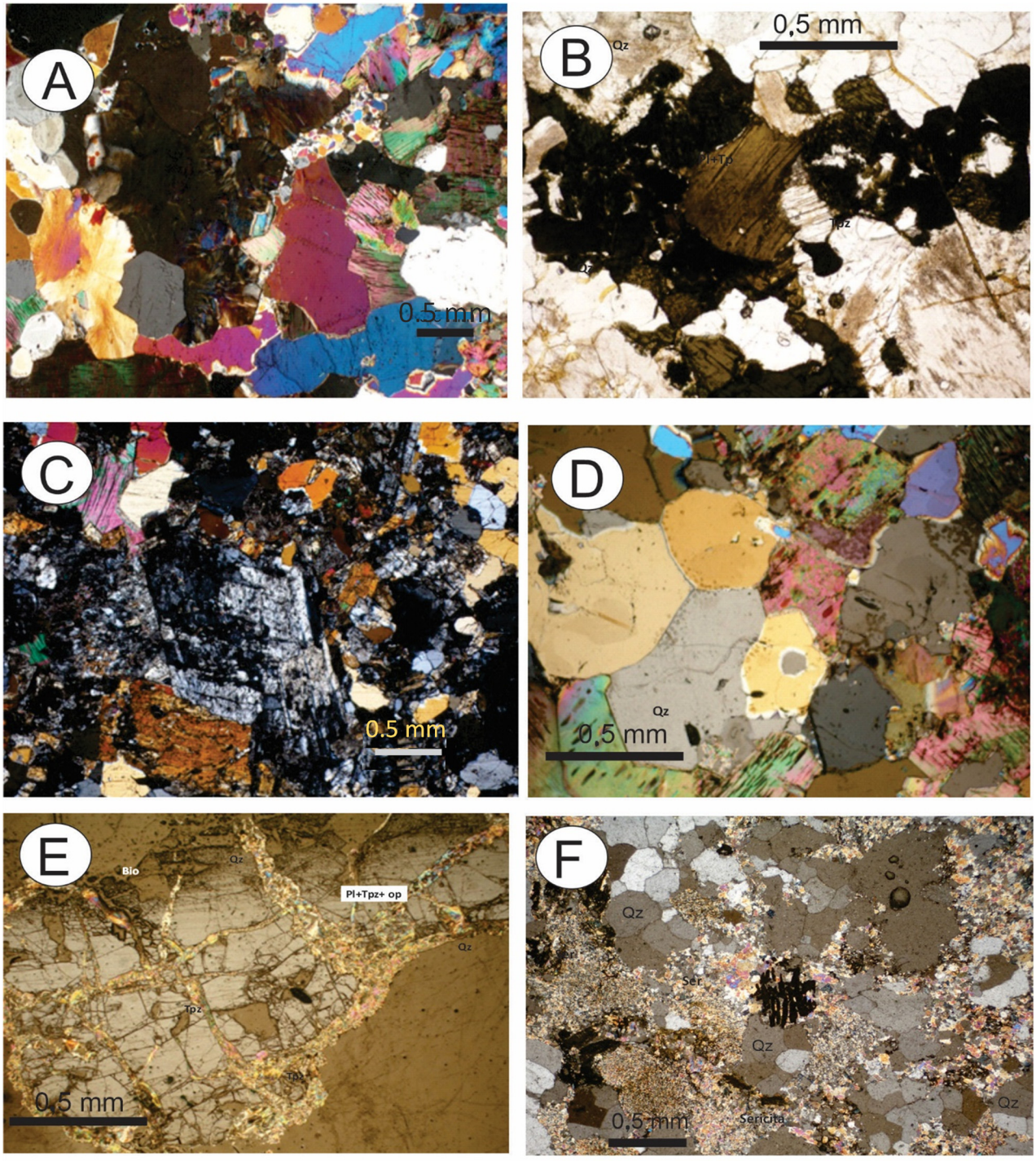

Figure 12. Macroscopic aspect of the albite-granite topaz. (**A**) Microscopic appearance of alkali-granite with feldspar with sericitic alteration in the center and with alteration crown at the edges in contact with microcline crystals. (**B**) Porphyritic gray syenogranite with feldspar veins shows microcline twin crystals in contact with anhedral quartz and biotite clusters. In (**C**,**D**) photomicrographs with parallel and crossed nicols showing beige to brown biotite clusters. In (**E**,**F**) photomicrographs with parallel and crossed nicols of well-altered biotite with inclusions of titanite and chlorite.

Quartz is also anhedral with sizes up to 0.4 mm and usually occurs in the interstices between the larger crystals of perthitic and albite feldspar; however, xenomorphic quartz phenocrysts with sizes up to 1 cm are also observed. The feldspars (Figure 12B) present are plagioclase (15%–25%) and microcline and/or orthoclase (30%–35%). Plagioclase is usually

interstitial and occurs in the form of short laths with a polysynthetic albite twin. Still, it can also appear in mega crystals (about 0.8 mm in length), constituting a microporphyritic texture. The microcline predominates to the detriment of orthoclase and occurs in the form of tabular crystals with polysynthetic twinning of albite and pericline. In some crystals, a perthitic texture is observed. Like albite, it sometimes forms larger crystals that characterize a microporphyritic texture. Orthoclase, when present, is anhedral to subhedral.

Alkali-granite facies

The secondary minerals are sericite, which occurs as a replacement product of plagioclase (Figure 11C), muscovite, and chlorite, which are products of alteration of K-feldspar and biotite, respectively. Reddish-colored Ti-oxide and orange Fe-oxide occur in fractures of more prominent minerals such as feldspars and quartz or as a replacement of biotite (Figure 12C). In some samples, precipitation of goethite is observed, that reflects the oxidizing conditions of the surface environment.

These rocks are associated with the biotite-granite described in an open pit mine presented in Figure 11D. In the outcrops, the alkali-granite is observed in contact with gneiss (Figure 12D), whose paragenesis consists of sericitized K-feldspar (Figure 12D), interstitial biotite deformity (5 to 15%), with pleochroism varying from beige to brown, and with serrated edges. In the second occurrence, the biotite has a more reddish color, changed to chlorite, and almost no longer shows extinction. It has pleochroic halos due to the inclusion of radioactive minerals such as zircon and monazite.

Alkali granite topaz

These pink-colored rocks (Figure 11E) are observed in contact with biotite-granite. They are composed of a fine matrix constituted by anhedral granular quartz and topaz in contact with orthoclase crystals and interstitial topaz (Figure 12E). In a hand sample, the biotite grains are about 1 mm, and the matrix, besides zircon as an accessory mineral, has other minerals (quartz + microcline + orthoclase). The biotite is green in color, with margins, and cleavage planes changed to chlorite; large grains of topaz are also observed (Figure 12F). (Figure 12F). In the northern portion of the São Domingos massif, the greisens develop associated with pegmatitic veins that occur both in contact with the gneiss and developed inside the granite, which is medium-grained and pink in color. The pegmatites and exogreisens will be characterized separately by presenting specific evolutionary features that may follow different evolutionary paths from the greisens.

The magmatic evolution of the endogreisens type B is shown in Figure 13. The endogreisens present coarse texture and mineral paragenesis with three compositional variations: Topaz-alkali granite, in contact gradual between alkali-granite and topaz-alkali granite. Following the magmatic fractionation, quartz-greisens consisting of >80% quartz, sericitized micas, and some feldspars are formed. The topaz-mica-quartz-greisens and quartz-mica-greisens have a balanced composition of quartz and micas varying between 60%–40% or vice versa. The micas are pinkish and light green (zinnwaldite, lithiniferous mica) and present in the cleavage filled with opaques and Ti oxide.

(C) Pegmatite and exogreisens

Pegmatites and exogreisens present similarities. The tabular form embedded in basement rocks is the main form and common feature between pegmatites and exogreisens. Figures 14 and 15 show topaz-zinnwaldite-pegmatites and exogreisens with their respective mineralogical compositions given by the slide images where topaz, zinnwaldite, and quartz are observed.

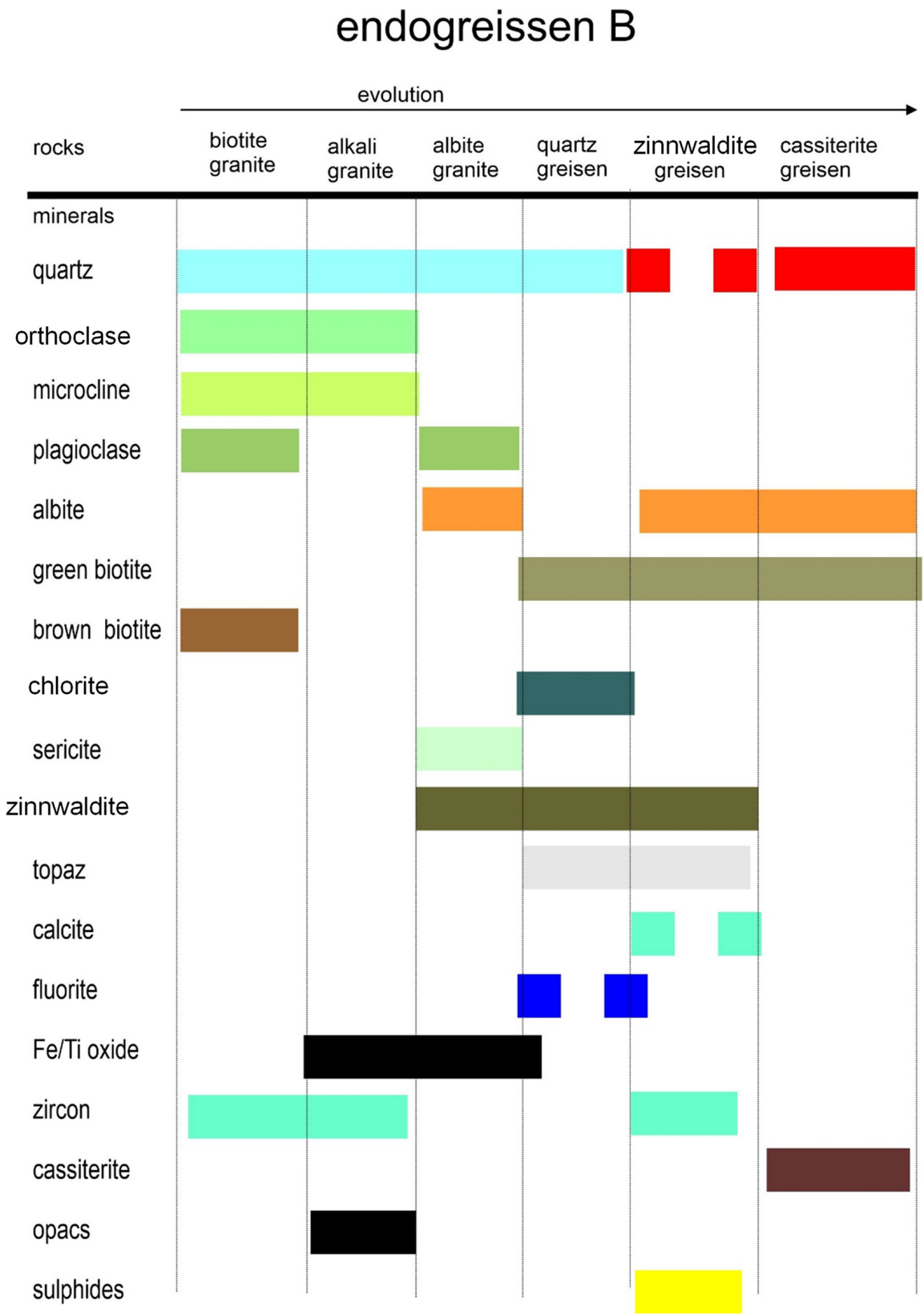

Figure 13. Mineral paragenesis was obtained by petrographic analysis of samples related to Endogreisen B. The petrographic studies indicate the magmatic-hydrothermal fluids evolved from biotite-granite to alkali-granite to topaz-granite, reaching the greisens phase. At the final evolution stage, the topaz-mica greisens are formed, composed of a hypidiomorphic matrix of topaz, zinnwaldite, and plagioclase and phenocrysts of topaz and quartz.

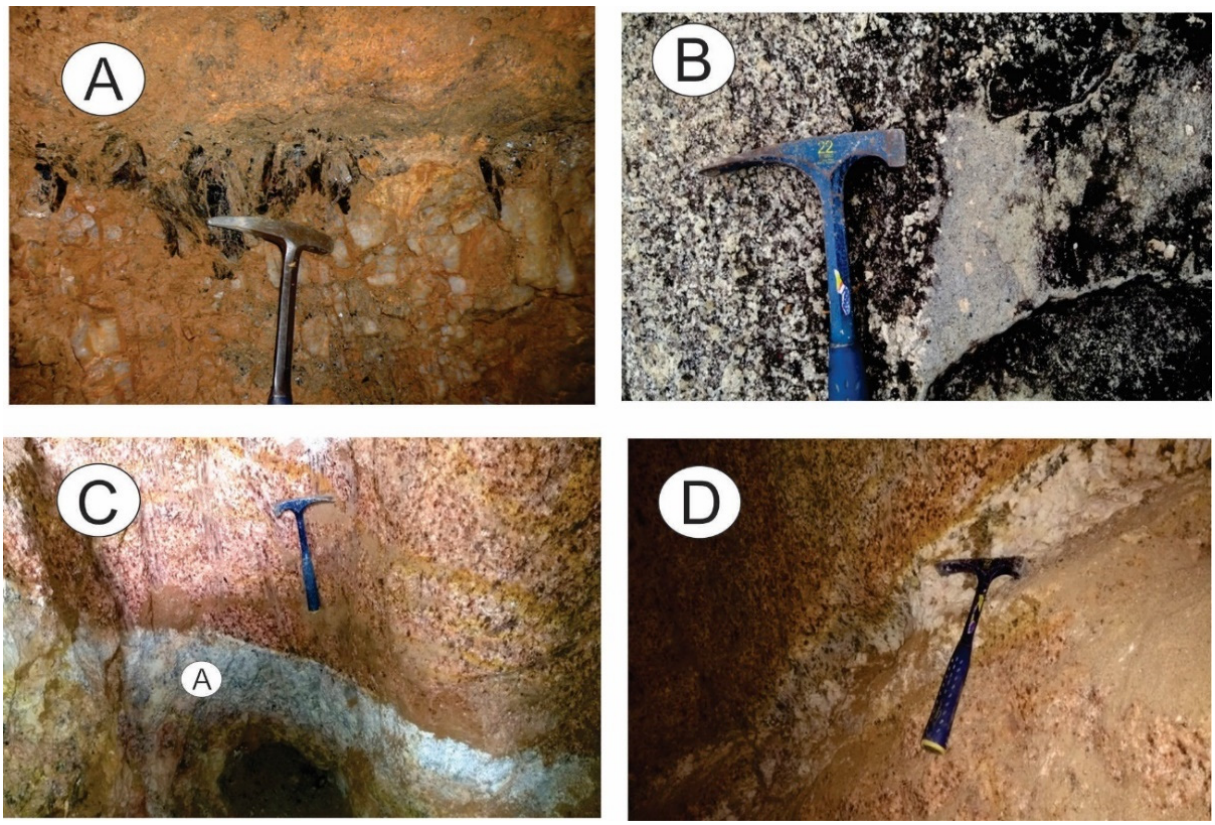

Figure 14. Macroscopic aspect of the exogreisens that make up the São Domingos Region. (**A**) Detail of the pegmatitic vein composed of K-feldspar, quartz, cassiterite, and zinnwaldite; (**B**) photomicrograph of exogreisens intercalated with a vein of quartz with cassiterite; and (**C**) contact between the quartz vein with cassiterite and; (**D**) the greisen zone with zinnwaldite development.

Pegmatites

A pegmatitic vein with N25E direction occurs in contact with lenses of medium to fine-grained pinkish granite (Figure 14A). This pegmatitic vein does not have sizeable internal zoning (Figure 15A) like the others described; it has a pinkish color due to a large amount of K-feldspar, followed by quartz, which varies from anhedral crystals among the mass of K-feldspar, with sizes from 1 to 5 cm, or in more quartzous portions of 30 cm thick. It is associated with agglomerates of greenish mineral (siderophyllite + cassiterite), in addition to biotite that presents in some lamellae a reddish color due to superficial oxidation. The vein appears to develop from fine granite (Figure 14B). In lamina, the cassiterite is black and occurs both in this green mineral mass and in the feldspars (Figure 15B). Spherical agglomerates of gray and white (very small) minerals also occur (Figure 14C), identified as a mass of lath-shaped cassiterite and siderophyllite. Other observed facies suggest feldspathization processes forming topaz-albite granites and topazification that compose the most evolved facies of the pegmatite (Figure 15C).

The petrographic analysis of pegmatite samples identified the following faciological variations. The first topaz-zinnwaldite facies is composed of rock with subhedral quartz and plagioclase in the form of slats that cluster in the interstices between the larger quartz crystals. In these facies K-feldspar is scarce and intensely sericitized, and mica and zinnwaldite are associated with opaques. The second topaz facies, here named siderophyllite topaz, consists of a pinkish to whitish colored rock with well-developed micas. Under the microscope presents a matrix composed of quartz, microcline, orthoclase, topaz, siderophyllite, and accessory minerals, such as zircon and opaque. The third facies is the topazine, consisting essentially of euhedral topaz crystals among a matrix of topaz + opaque and interstitial micas.

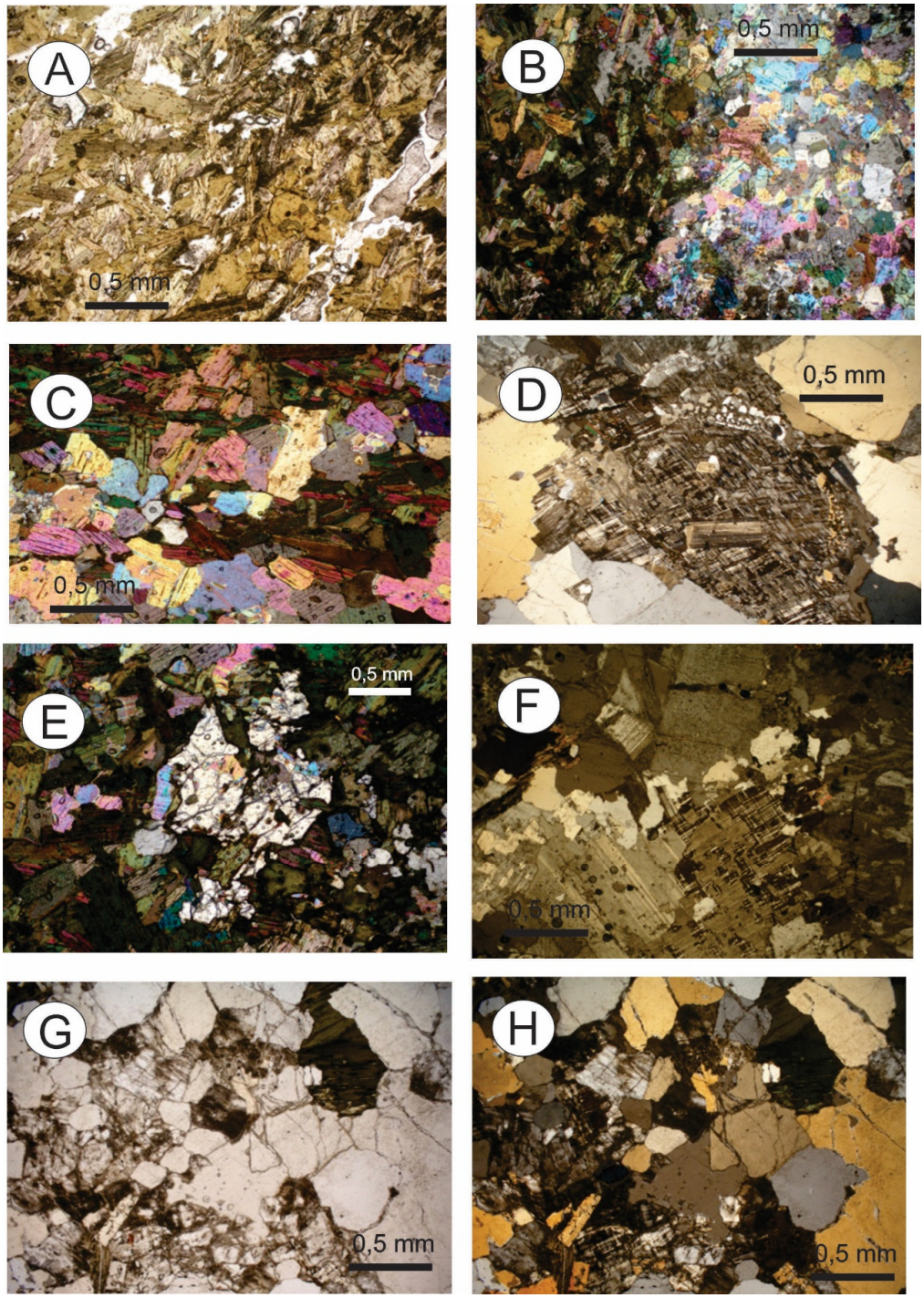

Figure 15. Microscopic appearance of the pegmatites and exogreisens associated with the alkali-granite observed in the São Domingos region; (**A**) Rock composed of quartz-sericite-greisen; (**B**) opaque minerals with sericitic mass bordering quartz crystals; (**C**) Detail of exogreisens minerals showing red coloration at the edges and white center, (interpreted as ilmenite); (**D**) quartz crystals in contact with zinnwaldite, quartz, and cassiterite. (**E**) topaz crystal fractured. among micas. (**F**), rounded quartz grains, green biotite, and interstitial microcline. (**G**) photomicrographs with parallel and (**H**) and crossed nicols: fine quartz, sericite, and cassiterite matrix.

Exogreisens

A significant occurrence of exogreisens is at the SW edge of the São Domingos Facies, where this mineralized body developed embedded in a thin gray gneiss. The host rock

presents fractures filled with milky quartz veins. These gneisses (Figure 14D) were dated and indicated to belong to the Serra da Providência Suite (1561 Ma; see U-Pb geochronology results below). Laterally this zone of veins of exogreisens developed in this gneiss is almost entirely chloridized and sericitized (Figure 15D), sometimes presenting brecciated portions with quartz fragments. The host rock is composed of a medium-grained pinkish gneiss composed of orthoclase, plagioclase, quartz, amphibole, and biotite (Figure 15E). Amphibole is dark green to brown, and orthoclase is anhedral shape (Figure 15F).

The exogreisens vary from green to gray and have mineralogy composed of quartz + zinnwaldite + topaz, with many associated opaque minerals and cassiterite (Figure 15G). The microscopic aspect of the exogreisens that make up the São Domingos region shows rocks made up of quartz-sericite-greisen with a sericitic matrix bordering the quartz crystals and opaque minerals (Figure 15H); ilmenite was identified as an opaque mineral in reflected light, showing a red color at the edges and white in the center.

In Figure 16, the magmatic-hydrothermal liquids had an evolution that suggests the direction from biotite-granite (and biotite) to alkali-granite to topaz-granite reaching the greisen phase (given by the pegmatitic texture) represented by the samples described as zinnwaldite-greisen, topaz-zinnwaldite greisen, and mica-greisen, as indicated by the mineral composition of each phase. Thus, the proposed evolutionary path has as its final stage a product composed of topaz-mica greisen, basically constituted by a hypidiomorphic matrix of topaz, zinnwaldite, and plagioclase and phenocrysts of topaz and quartz.

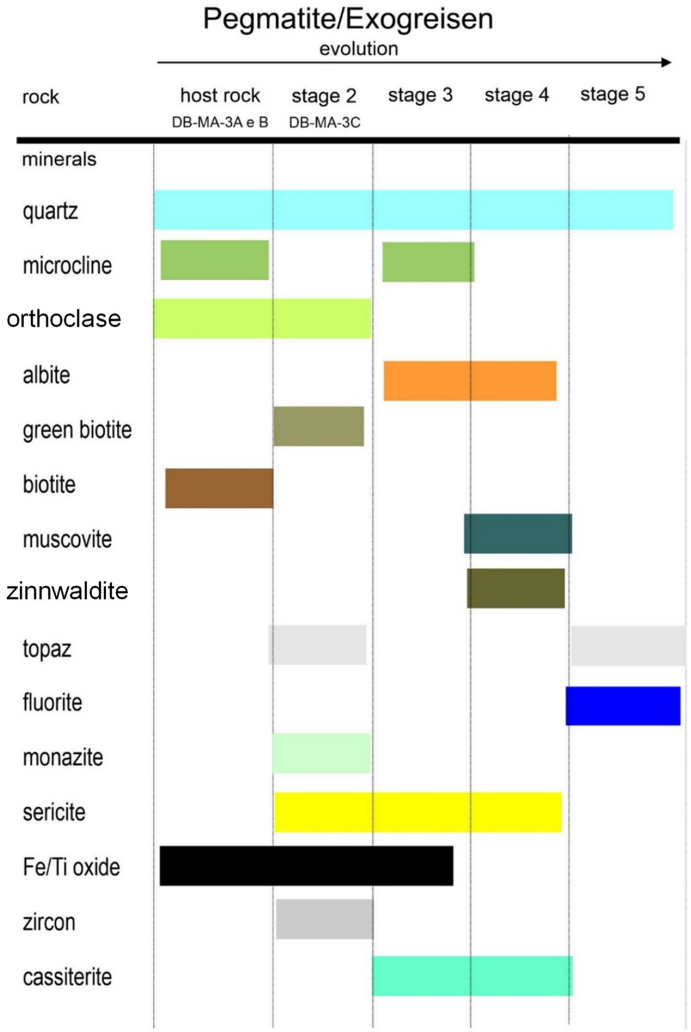

Figure 16. Mineral paragenesis was obtained by petrographic analysis of samples related to pegmatites and exogreisens.

6.2. U-Pb and Lu-Hf Geochronology

U-Pb zircon ages by LA-ICP-MS were obtained for four samples from the interior of Massangana granite. The analyzed samples aim to determine the ages of crystallization of granitic magmatism. The samples collected for U-Pb and Lu-Hf geochronology in this study are located at the southern end of the Massangana Granite, on the São Domingos Facies, where the mineralized areas are located (Figure 4). Scanning Electronic Microprobe (SEM) images of the analyzed zircon crystals from the Massangana Massif are presented for each sample (Figure 17), and the U-Pb analytical results are in Table S1 (Supplementary Material).

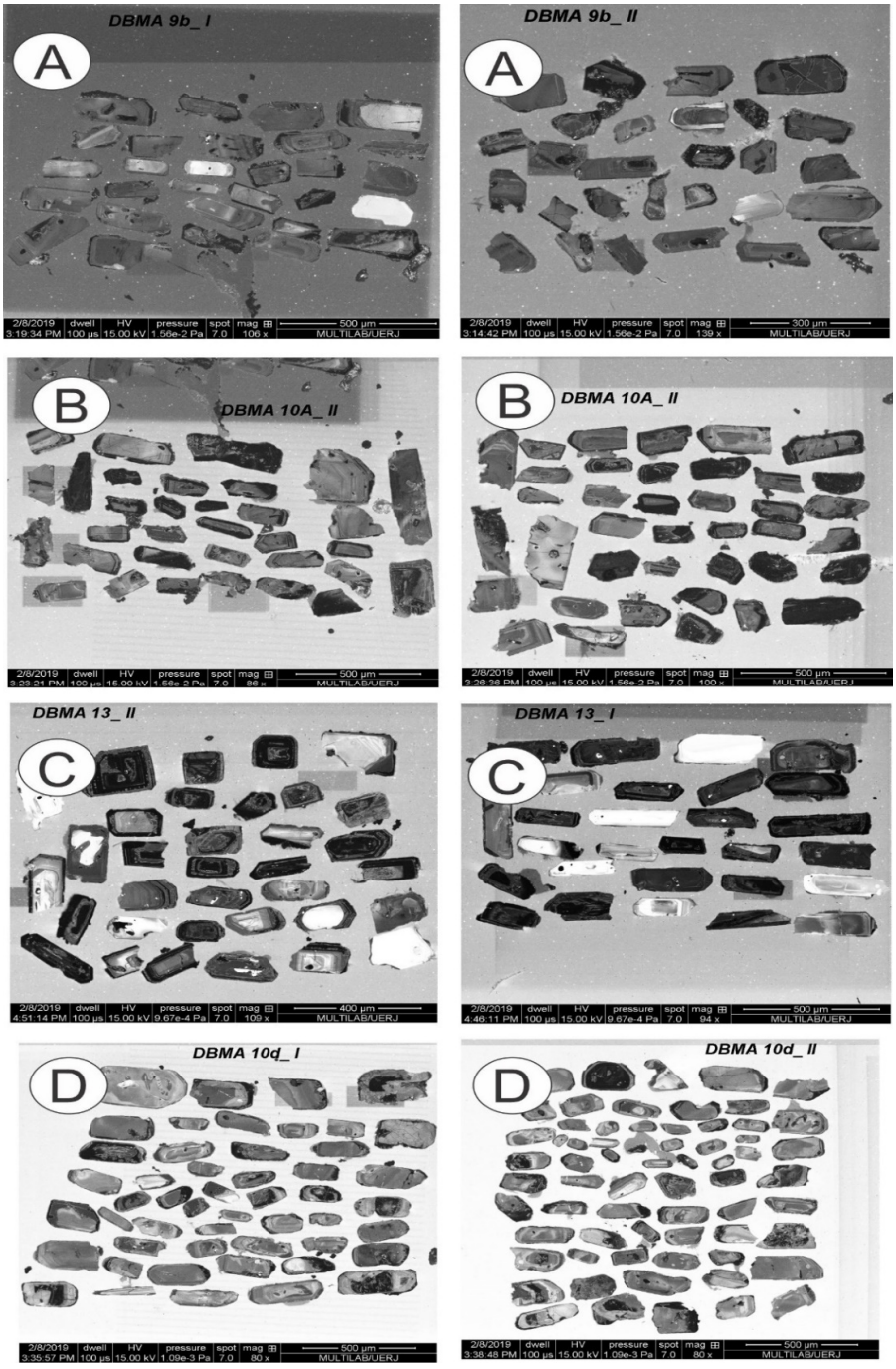

Figure 17. Cathodoluminescence images of zircon grains from samples: (**A**) DB-MA-9B; (**B**) BD-MA-10A; (**C**) BD-MA-32 and; (**D**) BD-MA-33.

Sample BD-MA-09, belonging to the evolution of endogreisens A, where the biotite-granite facies evolve to albite-granite and end in endogreisens, is composed of topaz-zinnwaldite-granite. The sample BD-MA-09 was collected in the mineralized portion of the São Domingos Facies and presents fine zircon prisms, with sizes that vary between 0.2 mm and 0.4 mm in length; some zircons are bipyramidal, others have rounded edges; zircon colors vary from transparent to pink and caramel (Figure 17A). Features such as oscillatory zoning are observed in most of the analyzed crystals; however, some crystals show a homogeneous aspect without zoning. Five spots were selected for making the Concordia curve (Figure 18A). All analyzes agree, with ratio values between 99 and 117%. The age obtained for sample BD-MA-08, interpreted as crystallization age, was 1081 ± 28 Ma.

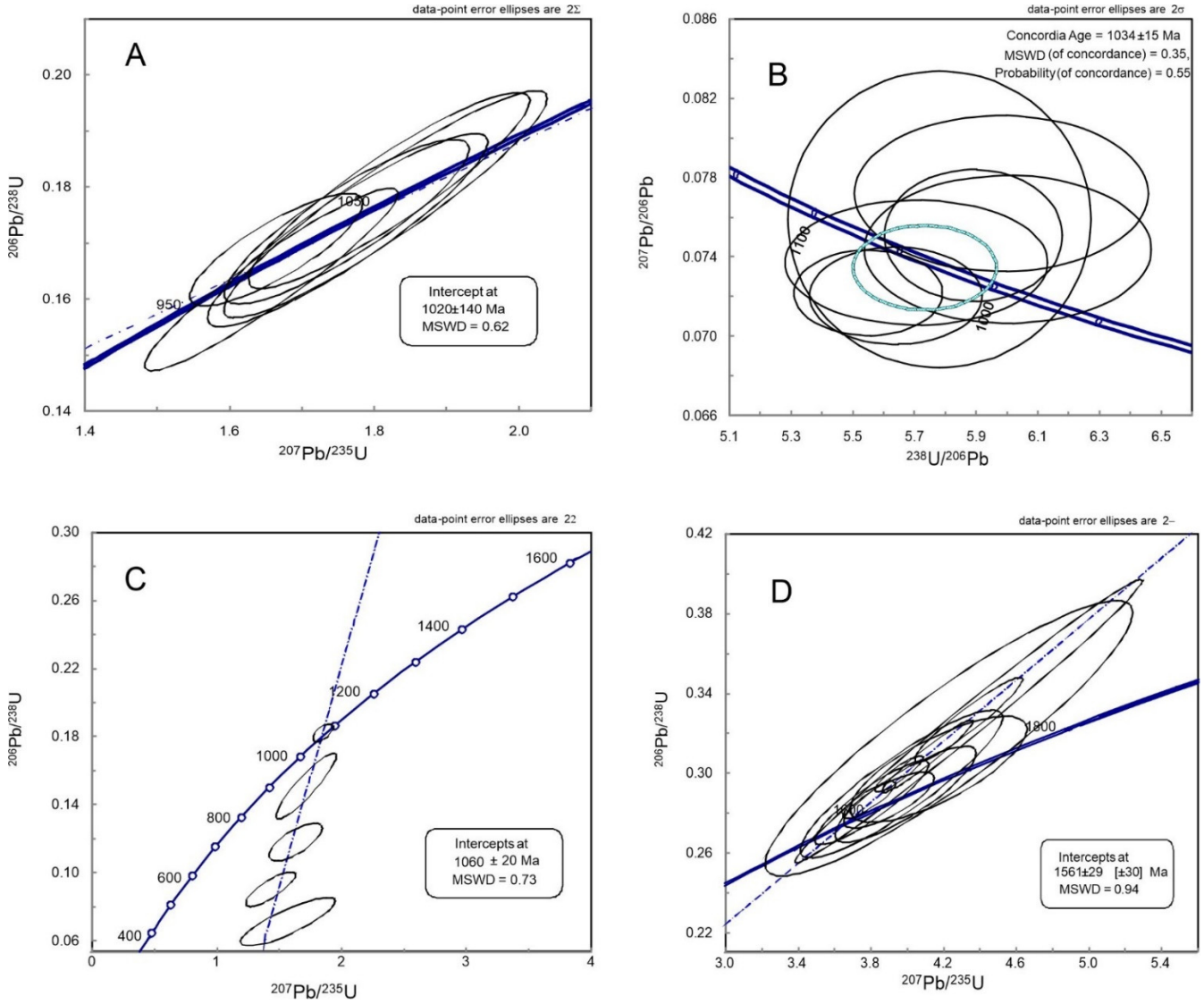

Figure 18. Concordia diagram of the analyzed samples in this investigation. (**A**) BD-MA-09B endogreisens sample collected at the São Domingos Facies in Massangana granite; (**B**) Concordia diagram of the representative sample of biotite-granite contained in the southeast portion of the Massangana Massif. The age obtained was 1060 ± 35 Ma; (**C**) Concordia diagram for BD-MA-13 endogreisens sample collected at the São Domingos Facies in Massangana granite; (**D**) Concordia diagram of the representative sample of gneiss from Serra da Providência suite. The obtained age, interpreted as the age of crystallization, is 1534 ± 15 Ma.

The second sample (BD-MA-10A) was collected in the southeastern portion of São Domingos Facies. The analyzed zircon grains range from elongated prisms (about 0.5 mm long) with bipyramidal ends, generally clear and without inclusions, to short grains (2–3 mm long) that may be euhedral or represent only part of the crystal. All dated crystals show oscillatory zonation, typical of igneous crystals (Figure 17B). Colors vary mainly from colorless to caramel; subordinately, pink crystals showing fractures occur. To plot the Concordia diagram (Figure 18B), fourteen spots were selected that show concordance values of the ratios between 98 and 104%. The age obtained for the BD-MA-10A sample, interpreted as crystallization age, was 1065 ± 38 Ma.

The BD-MA-13 sample, corresponding to a biotite-hornblende granite, was collected in São Domingos. The analyzed zircon crystals (Figure 17C) range from short (0.2 mm long) to elongated (0.6 mm long) prisms, both with bipyramidal ends. The crystals are clear, free of inclusions, and have a less marked oscillatory zonation than in the other samples. Colors range from light to dark caramel. Fifteen spots were used to make the Concordia diagram (Figure 18C), showing concordant values of ratios between 97 and 102%. The age obtained for the BD-MA-13 sample was 1034 ± 15 Ma, which was interpreted as crystallization age. The three samples analyzed presented results whose ages are compatible with the Santa Clara Intrusive Suite as shown by [59].

The BD-MA-10D sample is composed of a biotite-gneiss and was collected in the northeast portion of São Domingos Facies in the occurrence of endogreisens. The analyzed zircon grains are prismatic, ranging from 0.2 to 0.5 mm in length, usually with rounded and/or broken edges. Some grains show oscillatory zonation, while others are more homogeneous. The colors vary between colorless caramel, and pink (Figure 17D). To make the Concordia diagram (Figure 18D), seven spots showed concordant values between the ratios ranging from 97 to 103%. The age obtained for this sample was 1561 ± 30 Ma, representing the crystallization age.

6.3. Lu-Hf Isotopic Geochemistry

Four samples previously dated by the U-Pb method were submitted to Hf isotopic analysis. The values obtained for $^{176}Hf/^{177}Hf$ and the values of ε_{Hf} are presented below (see Table S2; Supplementary Material). The BD-MA-9B sample of biotite-granite composition have a crystallization age of 1081 ± 35 Ma, negative values for the εHf parameter, varying between −6.24 and −1.63, and a T_{DM} age between 1.77 Ga and 2.00 Ga.

The ε_{Hf} versus Age diagram is shown in Figure 19. The BD-MA-10A and BD-MA-13 samples, also of biotite-granite composition, with crystallization ages of 1060 ± 28 Ma and 1034 ± 15 Ma, respectively, present both negative and positive values for the parameter ε_{Hf}. For the zircon populations of the BD-MA-27 sample, the values of ε_{Hf} vary between −2.9 and −0.54 and between +0.31 and +1.95. The T_{DM} ages of these two samples were very consistent, ranging between 1.62 and 1.82 Ga, which indicates a predominantly Mesoproterozoic source. However, positive values were also obtained in all samples, indicating origins from melting crustal sources in different proportions, with a small contribution of juvenile material. The ages of mantle extraction (T_{DM}) obtained range from the Paleoproterozoic (2.40 Ga) to the Mesoproterozoic (1.52 Ga).

The T_{DM} ages between 2.65 and 2.06 Ga were observed in samples from the Massangana Massif before the formation of the rocks of the region, composed of rocks of the Jamari Complex (1.76 to 1.64 Ga) and must be related to deeper crustal sources, probably lower crust, of which no records have yet been found in the region.

The results obtained from the BD-MA023 sample with an age of 2115 ± 37 Ma suggest that the T_{DM} ages represent mixtures of crustal sources. Figure 19 shows the petrogenetic parameter ε_{Hf} versus U-Pb ages of the studied samples and the results obtained by [57] in granite samples from Massangana, Serra da Providencia, Santa Clara [58], and Alto Candeias granites [50]. In this sense, the Hf isotope evolution diagram for the set of results available in this investigation, added to the literature results, allows us to infer that the crust formation events in the Jamari Terrain can be grouped as follows.

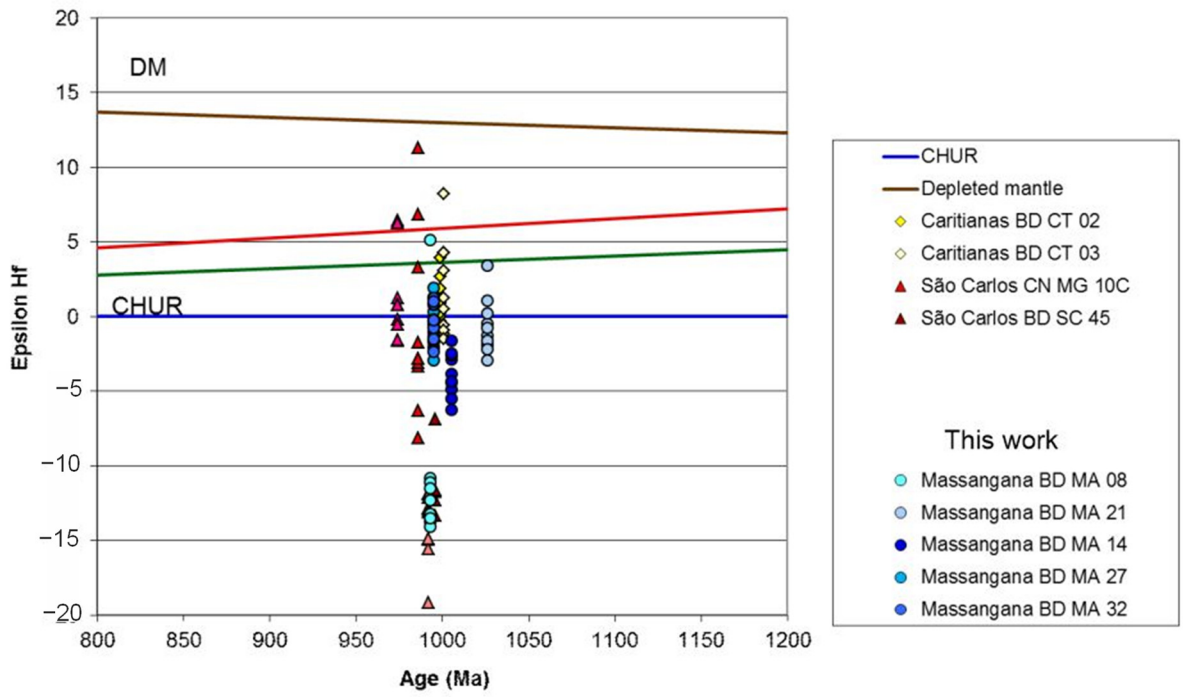

Figure 19. Diagram of the isotopic evolution of Hf for the granitic samples of the Rondônia Tin Province. The granitic samples show groups with Hf model ages indicative of periods of mantle extractions. The results show mantle and crustal sources for each magmatic pulse in forming magmas generating the intrusive suites.

The first group includes representative samples of the oldest model ages obtained by the Lu-Hf method, ranging between 2.8 and 2.4 Ga and negative ε_{Hf} values (−33 to −23). This group of rocks extracted from the mantle and lodged in the continental crust is represented today by part of the Serra da Providência, Alto Candeias, and Rondônia granites. These rocks present isotopic signatures of ε_{Hf} that also indicate positive values of ε_{Hf} and, thus, suggest bimodal sources (crust and mantle) for the origin of magmas. The vestige of these older rocks in the Jamari Territory does not present records in the literature and geological cartography of Rondônia. The lack of observations of this older crust may be related to the depth at which it is located, the lack of detailed mapping in the region, or due to the fact that crustal reworking processes have consumed this crust.

A second event with mantle extraction and lodging in the crust (Figure 19) occurred between 2.3 and 1.9 Ga, and isotopic traces are identified in the Serra da Providência, Alto Candeias, Santa Clara, and Rondônia granite rocks. These rocks present negative ε_{Hf} values (between −22 and −17). The third grouping of T_{DM} ages indicates the crustal residence of 1.7 to 1.3 Ga, with bimodality indicative of the mixing of the mantle and crustal sources for the formation of the respective magmas. Rocks represent the units that keep traces of this event from the Alto Candeias and Rondônia granites. The youngest continental crustal generation event does not have well-defined time limits, appearing to be between 1.2 and 1.0 Ga and represented only by rocks from the Younger Granites of Rondônia.

7. Discussion

7.1. The Petrogenesis of the Massangana Massif

Rapakivi granite intrusive suites in Rondônia Tin Province have been extensively studied in recent decades [49–59]. Despite being primarily anorogenic, new studies [62,63] have shown that distal relationships with orogenic events may play an important role in forming these suites. The bimodal character, which was previously only suggested, through petrographic and lithogeochemical features, with the advent of new isotopic analysis techniques, mainly the U-Pb geochronological and Lu-Hf isotopic data set in

zircon crystals, can now be corroborated. The union of these techniques has proven to be an essential tool in the source definition of the rapakivi granites.

Type A granites, mainly when fractionated, are melted with low viscosity due to their high temperature, moderate H_2O content, and high fluor content. This is consistent with the interpretation of other authors [64,65] who have investigated the origin of granites in the Rondônia Tin Province. The most critical point is to define what the lower crust was. The isotopic data indicate primary rock extraction ages ranging from the Paleoproterozoic to the Mesoproterozoic, showing that there was a mixture of different crustal sources in the formation of the granites that make up the Rondônia Intrusive Suite.

Massangana granite cassiterite, wolframite, and columbite-group mineral deposits exhibit similar features to the Kivu Belt tin granites, as reported by [66]. This belt has many occurrences of economic interest associated with the G4 granitoid intrusions that were emplaced between ca. 1050 and 970 Ma in the Mesoproterozoic Kibaran Belt of Central Africa, which contains mineral deposits, such as beryl, amblygonite, spodumene, apatite, and tourmaline.

Considering the data obtained in this study and the literature, it is suggested that: the massifs studied in this investigation, belonging to the Rondônia Intrusive Suit or Younger Granites of Rondônia, evolved from two or more distinct sources; each massif may have had an evolutionary history characterized by partial crustal and mantle melting processes, associated with magmatic mixing and fractional crystallization processes.

The partial melting of sources for type-A granites requires, according to [2,67,68], a large amount of heat. However, rocks classified as anorogenic generally occur in stable and cold regions of lithospheric thickening. According to Black [9], the entrance of heat, regardless of its origin, results in erosion and/or mechanisms of delamination of the lower lithosphere. The proposed possible scenarios resulting in lithosphere delamination involve heat coming from mantle plumes or through movements along shear zones. In the case of rocks from the Rondônia Intrusive Suite, the hypothesis of a combination of crustal sources (dominant) with mantle sources from a crustal extension that resulted in crustal melting, magmatic mixing, and fractional crystallization seems to be the adequate model.

7.2. Geochronology of the Massangana Massif

It is difficult to accurately determine the distribution of the lithofacies in the Massangana Massif, the most complex of all because a large part of the central-west portion of this massif had low sampling density. The area corresponding to the Bom Jardim and Taboca magmatic phases, delimited by [59], has a higher sampling density due to the exposure of rocks in the mining fronts. However, it is possible to verify that the biotite granites occur preferentially at the edges of the massif, while the biotite hornblende granites occur in the most central portions.

Porphyritic rocks (pyterlites) occur in the north-central (sample BD-MA-34) portion at biotite-granite facies and south-central (sample BD-MA-28) part at the biotite-hornblende-granite facies. The samples that correspond to the São Domingos phase by [59] are predominantly biotite-granites, and the medium and fine-grained types (Taboca Phase) occur intruded in the coarse to porphyritic facies, both in the Massangana and in the Saint Domingos phase.

The U-Pb results reported here can be evaluated in conjunction with literature data. In this way, the results complement each other, showing the variety of ages of the rocks enclosing the Massangana Granite and the homogeneity of ages obtained for this intrusion. Figure 20 shows the ages of [57] with U-Pb ages between 1026 and 974 Ma, indicating polycyclic magmatic processes that incorporated crystallized host rocks 1561 $\pm$ 29 Ma (Serra da Providencia Suite).

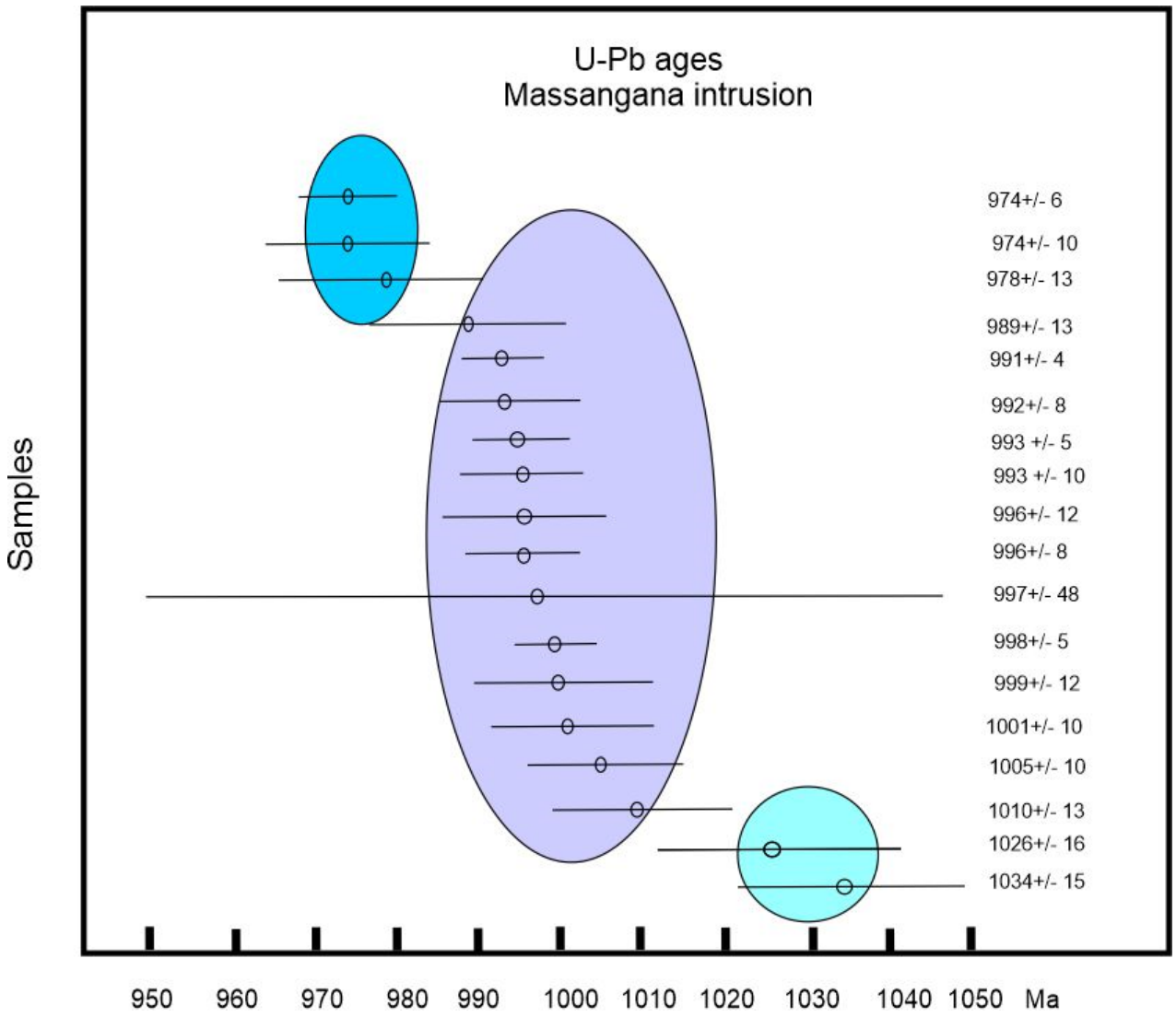

Figure 20. U−Pb ages of the Massangana Massif samples. Distribution diagram of the U−Pb ages in zircon, except for one monazite (997 ± 48 Ma) from the granites of the Rondônia Tin Province. Source: [19,57].

The only sample collected in the Massangana Massif with age consistent with the crystallization of this unit is represented by the sample BD-MA-13. It provided a period of 1034 ± 15 Ma and represented a biotite-hornblende granite collected in the region of São Domingos. This age is compatible with the crystallization ages of the Massangana Massif, as reported by [19,57].

Two other samples provided ages of 1081 ± 28 Ma (BD-MA-08) and 1065 ± 38 Ma (BD-MA-10A), interpreted as crystallization ages compatible with the Santa Clara Intrusive Suite as presented by [58]. The U-Pb results reported here (Table S1; Supplementary Material) show an ages range of the rocks enclosing the Massangana granite due homogeneity of ages obtained for this intrusion. As reported by [58], the results of the U-Pb geochronological analyzes performed on zircons from the Massangana Massif were: 998 ± 12 Ma for the biotite-granite of the São Domingos phase; 995.7 ± 9.5 Ma, 1005 ± 10 Ma and 1010 ± 12 Ma for the Massangana-phase biotite granites and; 1026 ± 16 Ma for the hornblende-biotite granite, also correlated to the Massangana phase [47].

The U-Pb ages obtained for the São Carlos Massif [46] are 986 ± 14 Ma and 974 ± 10 Ma for samples of the alkali-granite facies collected in the central portions of the massif, and 992.5 ± 7.7 Ma and 996 ± 8 Ma, for samples of alkali-granite and biotite-granite fa-

cies, respectively. For the Caritianas Massif, the ages obtained were: 999 ± 12 Ma and 1001 ± 9.8 Ma for the biotite granites. The first was collected in the most southeastern portion of the massif, and the second was in the most central part.

The ages obtained in this study agree with the ages reported by [57] for the massifs: São Carlos with 995 ± 73 Ma and 974 ± 6 Ma, and Massangana, with 991 ± 4 Ma. The ages obtained for the Massangana Massif show a wide variation in the crystallization period (about 30–40 Ma). Thus, it is suggested that at least two magmatic pulses were responsible for forming the Massangana and São Domingos phases, the former being the oldest in the granitoid complex, as [57] had already suggested.

Figure 20 shows the age distribution (with the respective errors) of each sample from the Massangana Massif obtained in this work and the literature. In this diagram, it is possible to suggest the existence of three groups of samples; the first presents only two samples, with ages between 1034 Ma and 1026 Ma. A second group, with ages between 1010 Ma and 997 Ma, represents the most significant number of samples analyzed. The third group represents the youngest ages, with only three samples, with ages between 978 Ma and 974 Ma. The errors associated with each dated sample suggest that the rocks of each group do not present superposition, so even with the errors, the three groups are significantly separated and may be representative of distinct magmatic pulses in the magmatic evolution of the Massangana Massif. It is also observed that the group of rocks with younger ages is not related to tin mineralization.

7.3. Hf Isotopes from the Massangana Massif

Hf isotopes allow the investigation of a wide range of geological questions to be addressed, such as what rate of magmatic addition of the mantle to the crust or how the source of magma (such as mantle isotopic evolution) changes over time. Furthermore, due to the ability to delineate the main geological features of the crust, the spatial relationships in isotopic signatures can have important metallogenic implications.

Generally, Hf zircon ratios yield a range of isotopic values, despite being from a single igneous sample with a single U—Pb crystallization age [69,70]. This variation in composition can be explained by an imbalance of magma composition or by a mixing of magmas [71–74].

Regardless of the petrological reason for the wide range of ε_{Hf} compositions in zircon in a single magma system, visualization of such data cannot generally be effectively accomplished by simple arithmetic, geometric, or weighted average.

In general, the mantle extraction ages (T_{DM}) obtained for the zircon grains of the sample BD-MA-08, belonging to the São Domingos phase [59], shows values from the Paleoproterozoic, higher than those of the other samples of this massif (between 2.40 and 2.24 Ga), which indicates the involvement of older crust in the formation of rocks in this portion of the Massangana Massif, which, despite having petrographic aspects and crystallization age very similar to the rocks of the Massangana phase, are originated from a different crustal source.

The T_{DM} ages of the BD-MA-10A sample from the São Domingos phase show only Paleoproterozoic values (between 2.40 and 2.23 Ga), except for one zircon that presented a T_{DM} age of 1.30 Ga. The ε_{Hf} of this sample has the most negative values (between −14.1 to −10.8), except for the same zircon that showed a positive value for ε_{Hf}. These data, associated with the age of crystallization, indicate that the magma related to this sample from the São Domingos phase must have crystallized from an older source than those from the Massangana phase, represented by the other samples that have T_{DM} age values between 1.85 and 1.52 Ga and ε_{Hf} values ranging from negative (−6.2 to −0.2) to positive (+0.2 to +3.4) showing a mixture of crustal and mantle material in the formation of these rocks.

The significant variation in ε_{Hf} values indicates source heterogeneity in the Massangana, Caritianas, and São Carlos massifs, representing predominantly crustal melts with a subordinate contribution from the mantle. The Caritianas Massif, which presented a more positive value for the ε_{Hf} parameter, seems to have had more contribution from the

mantle than the other massifs studied in this work. Thus, mineralization suggests that it is associated with the participation of the older crust in the generation of magmas that gave rise to the process of fractionation and enrichment of noble metals. Characterizing sources of rapakivi rocks can play an essential role in the genesis of cassiterite ore and can represent an essential tool for mineral exploration.

7.4. Two Observed Magmatic Suites

Greisens described in this work may be associated either with rocks rich in albite (sodium) or with rocks rich in alkali feldspar (potassium). These mineralized bodies in this investigation were also described as topaz-granites and are generally located on the margins and the ceiling of granitic intrusions or close to contacts with the host rocks in the form of small stocks or dykes. The main mineralogy of topaz-granites is composed of albite (Or_0–Or_{10}, An_0–An_4), usually in euhedral crystals, K-feldspar (usually microperthite or orthoclase microcline), and lithiniferous mica (zinnwaldite).

Corroborating the observations reported here describing two types of ore (one related to albite-granite and the second to alkali-granite), the Rondônia Granites were subdivided by [75] two distinct suites. The first is composed of metaluminous to marginally peraluminous and sub-alkaline subsolvus with associated minor quartz-syenite, quartz-monzonite, and monzonite, and the second shows alkaline affinity. Field relationships suggest that alkaline rocks are younger than sub alkaline types.

The alkaline suite is composed of alkali-feldspar granite peralkaline, and alkali-feldspar granite, and consists of at least three distinct phases of intrusive granite. The first intrusive bodies are coarse pyterlitic to porphyritic biotite syenogranite, with late intrusive syenogranite and alkali-feldspar granite predominating. Recent intrusive rocks are rare and mainly comprise albite-mica-(topaz) granite. Deposits of primary tin and associated metals are spatially related to the granites of the last two phases.

(A) Suite with sodification (albitization)

The evolution of mineral paragenesis can be interpreted as a variation of a highly complex zoning framework, where the gains and losses of elements strongly depend on the location of a rock sample in a specific metasomatic zone. However, general rules can be derived from the results of various calculations of chemical changes between altered and unaltered rocks by many authors. First, due to the reaction of plagioclase and alkali feldspars, sodium is significant and has constant release. Likewise, potassium can be gained or lost depending on the mica content of the rock. At the same time, silica and alumina can be obtained or lost, depending on the mineral changes in the greisen: in quartz-rich greisens, silica is acquired; in mica and topaz-rich greisens, alumina can be increased.

The decrease in the viscosity and density of the residual melt due to the increase in the F content, according to [76–78], facilitates fractional crystallization processes of albite-rich granites in F. The increase in F seems to also be related to the concentration of F incompatible elements (including metals of economic interest) in residual castings. Therefore, adding F can increase the Si/(Si + Al) ratio and the SiO_2 activity in the magma and, at the same time, increase the activities of the $NaAlSi_3O_8$ component. This process is indicated for a group of samples reported here and grouped in the evolution diagram of mineral paragenesis presented in Figure 21, where the less evolved representatives are biotite-granites and albite-granites. Topaz-granites represent the intermediate stages with zinnwaldite and lithiniferous micas that end the evolution with products where the feldspars were replaced by topaz (generating topazites).

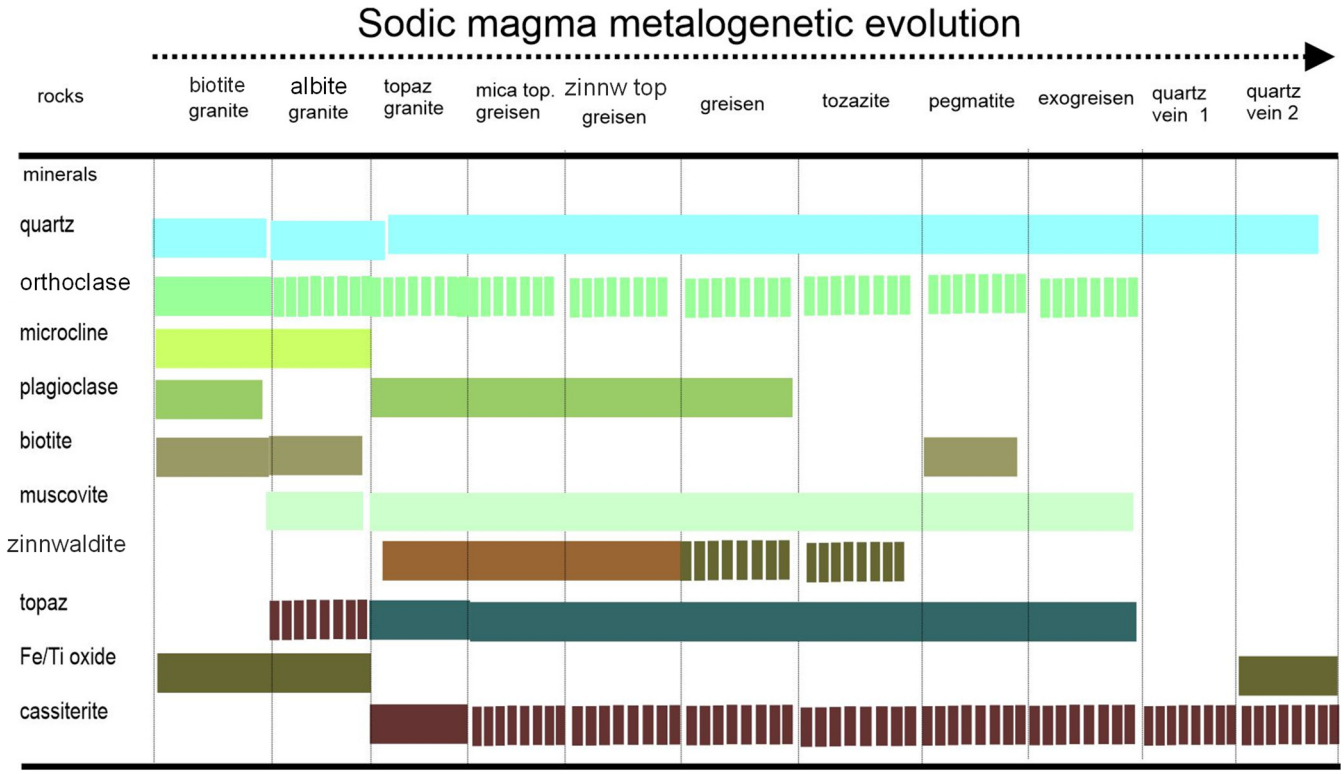

Figure 21. Paragenetic evolution of mineralized Massangana Massif rocks. The development of sodium magma and hydrothermal solutions is responsible for mineralizing rare metals in the Massangana Massif.

Under the condition of high F content (F = 6% by weight), all AlO_2 tetrahedra should have been destroyed and the feldspar should have been, by topaz, crystallized from this F-rich magma [70]. Thus, petrographic analyses suggest that the fractionation between the fluid phase and the residual magma results in the loss of alkali, while metasomatism occurs, which may have led to the enrichment of rare metals in multiple stages. Due to the high chemical imbalance, this fluid phase may have reacted with the host granite in structural traps, with the consequent precipitation of cassiterite.

(B) Potassic Suite (alkalinization)

In tin granitic provinces, although most of the alkaline plutons are predominantly composed of coarse- to very coarse-grained biotite-monzogranites or porphyritic with K-feldspar mega crystals, including rapakivi rocks, a large textural variation is expected in the apical and marginal zones of the granite plutons [71].

This variation is represented in the São Domingos phase by microgranites to porphyritic granites passing through medium granites intruded into the coarse-grained granites in the form of dykes. These rocks have more evolved chemistry than their parent granite host (biotite-granite) and may even evolve to pegmatitic facies, including endo- and exogreisens and mineralized quartz veins, as suggested in Figure 22, where rocks mineralized into rare metals are a result of fractionation of alkaline granitic protoliths.

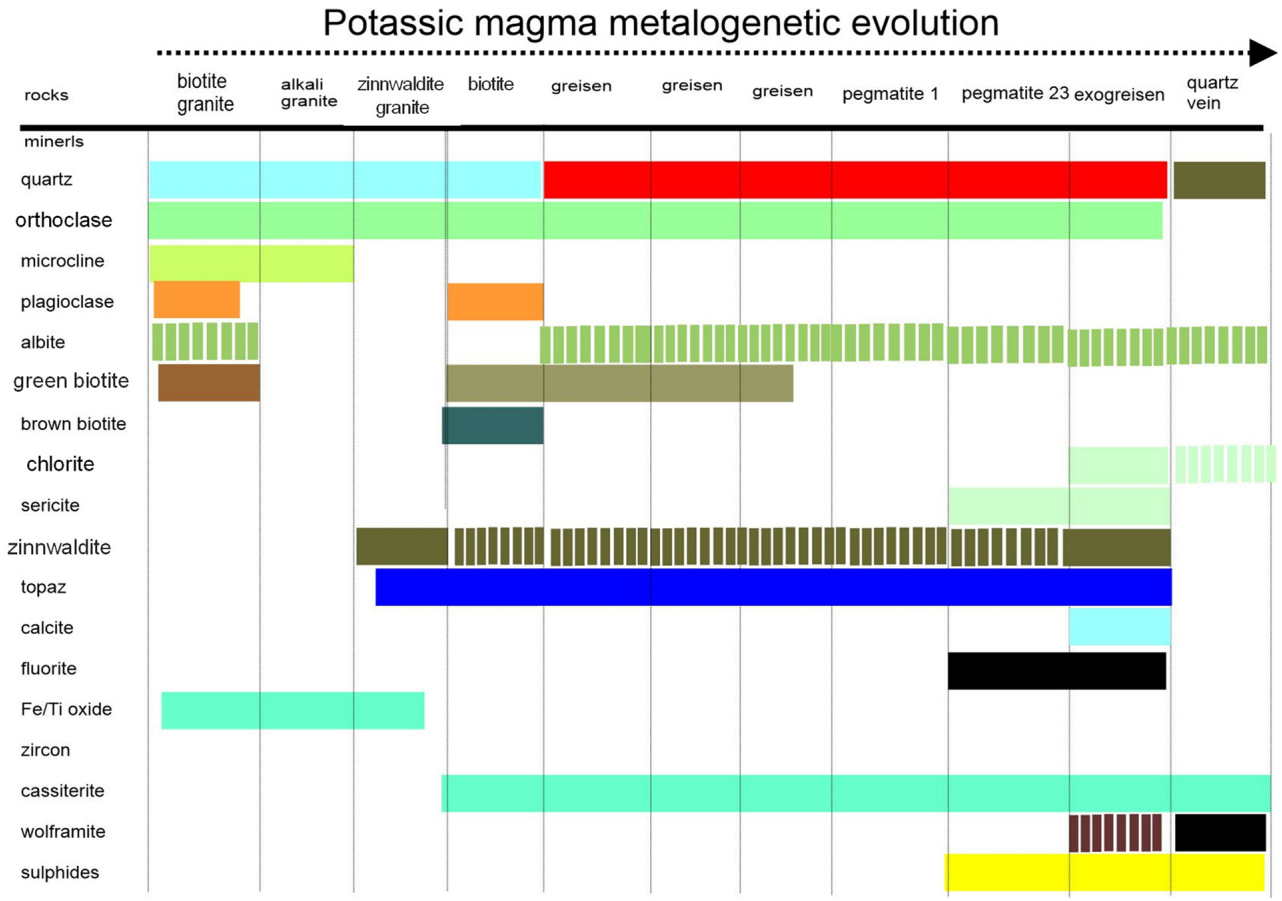

Figure 22. Paragenetic evolution of mineralized Massangana Massif rocks. The evolution of potassium magma and hydrothermal solutions is responsible for the mineralization of rare metals in the Massangana Massif.

7.5. Proposed Model

The evolutionary model (Figure 23) of mineralized bodies consists of rocks resulting from magmatic fractionation and metasomatism processes involving hydrothermal phases possibly exsolved from the original magma, with or without the contribution of meteoric waters. In this sense, the following stages of rock evolution were identified according to mineral paragenesis: (1) hornblende granites; (2) coarse-grained biotite granites to porphyritic biotite granite; (3) alkali feldspar-biotite fine granites; (4) fine quartz-syenites enriched in Nb and light REEs (5) topaz zinnwaldite granite; (6) topaz-granite and albitized granites; (7) K-feldspar and albite pegmatites; (8) endo and exogreisens and; (9) quartz veins with cassiterite and veins with topaz, beryl, and cassiterite. The first four sequences refer to essentially magmatic processes; the last four refer to processes that include post-magmatic alteration stages related to greisenization, including processes of albitization, topazification, and silicification.

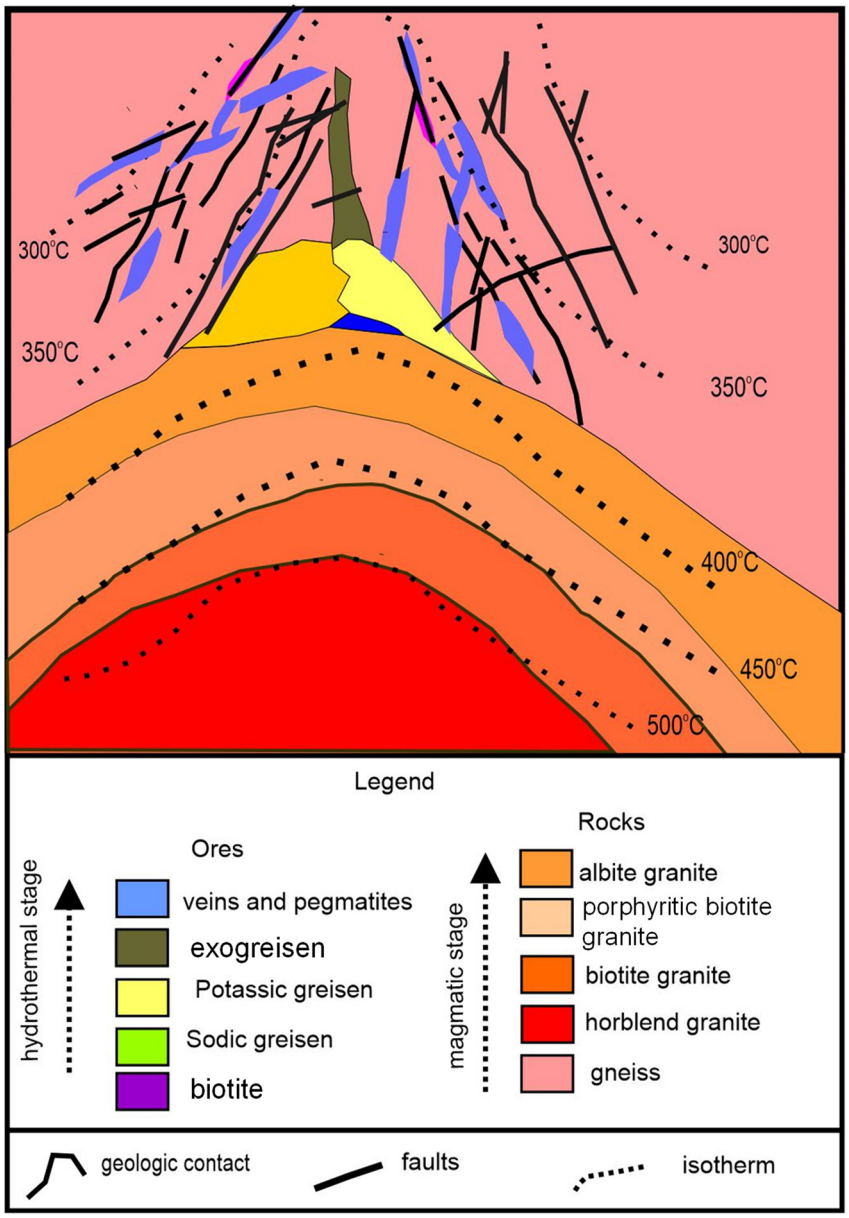

Figure 23. Schematic model of the rocks and fluids responsible for generating rare metal mineralizations in the Massangana Massif.

8. Conclusions

Proterozoic anorogenic granitic complexes commonly show chemical and petrographic features typical of tin granites, in many cases (Fennoscandia, Amazônia, and Rondônia) mineralized in Sn-W-Be-Zn-Cu. Based on the petrographic and isotopic U-Pb and Lu-Hf analyzes of this study and the literature, it is possible to reach the following conclusions:

(1) The Massangana Massif granites show typical characteristics of tin granites, with high (F, Li, Rb, Ga, Sn) and Nb and low (Mg, Ti, Ba, Sr, Zn, and Eu). Most lithotypes studied are characterized by subsolvus reactions that include alkali feldspar exsolution, recrystallization, and mineral alteration. The presence of a perthitic to mesoperthitic texture in the K-feldspars and of minerals such as topaz and fluorite in the accessory phases indicates the percolation of F-rich fluids and late or post-magmatic alteration processes.

(2) The geochronological data of the Massangana Massif reported here confirm the fractional crystallization (U-Pb ages of 1026 to 1005 Ma) with coarse to porphyritic

granitic facies, typical of slow cooling and, towards the south and southwest portion of the massif type medium granulation presents younger ages (995 and 993 Ma). The youngest ages are in the São Domingos massif and the southern portion of the Massangana Massif and correspond to the areas of primary ore occurrence, showing that granitoids with periods greater than 998 Ma are not directly related to the mineralized zones.

(3) The variation of values for ε_{Hf}, between positive and negative, with the predominant negative values, indicates a mixture of crustal sources (predominant) with mantle sources. The petrographic data also shows the occurrence of an intense process of magmatic fractionation related to the melting of crustal material. The primary mineralizations of the Massangana Massif are concentrated in the contact zones of the São Domingos granitic pluton with the gneissic rocks and fractures characterized by intense percolation and silica precipitation. In the central-west portion of the Massangana Massif, cassiterite occurs associated with beryl and sulfides (galena and sphalerite) in a widespread manner in the medium granite, the latter in contact with a biotite-granite intensely affected by the action of F-rich fluids, have almost wholly destabilized the feldspars, which give rise to topaz associated with metals and sulfides.

(4) The mineralization styles are (1) stockwork type with the dissemination of subparallel quartz veins with associated cassiterite and wolframite, which follow the main NE direction, corresponding to the main lineaments observed in several massifs of the Rondônia Stanniferous Province, (2) vein and venule systems with associated topaz, beryl, and cassiterite, (3) pegmatitic veins housed in both gneiss and granite, and (4) greisens disseminated in the form of blocks and pockets developed in *medium-grained* biotite granite and alkaline granites.

(5) The role of fluorine in modifying primary minerals is suggested, but its role in the deposition of cassiterite must be better understood. The presence of fluorine in the granitic system decreases the viscosity and density of the residual melt resulting in the formation of F-rich albite granite melts. At the same time, H_2O saturation produces an aqueous fluid where the paragenesis albite + K-feldspars + quartz + topaz + mica crystallizes. In this way, the decrease in the viscosity and density of the residual melt due to the increase in the F content facilitates fractional crystallization processes of albite-rich granites in F. While the saturation in H_2O produces an aqueous fluid with albite-K-feldspar-quartz-topaz-mica. The increase in F also seems to be related to the concentration of incompatible elements (including metals of economic interest) in residual castings.

(6) Massangana mineralized systems developed in the final stages of crystallization from highly fractionated magma. The addition of F to the system in the final stages of crystallization reduces the stable temperature of hydrated granitic magmas, destabilizing the feldspars and increasing the stability of quartz and topaz so that in the most evolved facies, the feldspars in the granitic matrix are replaced by quartz and topaz, forming the topaz granites and topazites and economic concentrations of Sn, W, and Ta.

Supplementary Materials: The following are available online at https://www.mdpi.com/article/10.3390/min12101304/s1, Table S1: LA-ICP-MS U-Pb results in zircon grains from the samples BD-MA-9b, BD-MA-10a, BD-MA-13, and BD-MA-10d, Table S2: LA-ICP-MS Lu-Hf results in zircon grains from the samples BD-MA-9b, BD-MA-10a, BD-MA-13, and BD-MA-10d.

Author Contributions: Conceptualization: B.P.D. and M.C.G.; methodology: B.P.D. and M.C.G.; formal analysis: B.P.D. and M.C.G.; resources: M.C.G., B.P.D., G.L.P., A.D.T.J. and M.V.A.M.; writing—review and editing, B.P.D., M.C.G., G.L.P., A.D.T.J. and M.V.A.M. All authors have read and agreed to the published version of the manuscript.

Funding: This research received no external funding.

Data Availability Statement: Data used in this work is available.

Acknowledgments: This work received financial support from Conselho Nacional de Desenvolvimento Científico e Tecnológico of Brazil, CNPq (project process # 443662/2018-5 and # 302676/2019-8) and Fundação Carlos Chagas Filho de Amparo à Pesquisa (FAPERJ) do Estado do Rio de Janeiro, Brazil (process #E-26/202.927/2019 and #E-26/211.278/2021). The authors would like to thank the reviewers and the Editor for their contributions, which significantly improved the initial version of the paper.

Conflicts of Interest: The authors declare that they have no conflict of interest.

References

1. Pitcher, W.S. Granite: Typology, geological environment and melting relationships. In *Migmatites, Melting and Metamorphism*; Atherton, M.P., Gribble, C.D., Eds.; Shiva Publishing Ltd.: Cheshire, UK, 1983; pp. 277–285.
2. Douce, A.E.P. Generation of metaluminous A-type granites by low-pressure melting of calc-alkaline granitoids. *Geology* **1997**, *25*, 743–746. [CrossRef]
3. Middelaar, W.T.V.; Keith, J.D. Mica Chemistry as an indicator of oxygen and halogen fugacities in the Cantug and other W-related granitoids in the North American Cordilhera. In *One-Bearing Granites Sytems: Petrogeneis and Mineralizing Processes*; Stein, H.J., Hannah, J.L., Eds.; Geological Society of America: Boulder, CO, USA, 1990; Special Paper 246.
4. Lehmann, B. *Metallogeny of Tin*; Lectures Notes in Earth Siences; Springer: Berlin, Germany, 1990.
5. Frost, B.R.; Barnes, C.G.; Collins, W.J.; Arculus, R.J.; Ellis, D.J.; Frost, C.D. A Geochemical Classification for Granitic Rocks. *J. Pet.* **2001**, *42*, 2033–2048. [CrossRef]
6. Frost, C.; Frost, B.R. Reduced rapakivi-type granites: The tholeiite connection. *Geology* **1997**, *25*, 647–650. [CrossRef]
7. Eby, G.N. Chemical subdivision of A-type granitoids: Petrogenetic and Tectonic Implications. *Geology* **1992**, *20*, 641–644. [CrossRef]
8. Batchelor, R.A.; Bowden, P. Petrogenetic interpretation of granitoid rock series using multicationic parameters. *Chem. Geol.* **1985**, *48*, 43–55. [CrossRef]
9. Frost, C.D.; Frost, B.R. On Ferroan (A-type) Granitoids: Their compositional variability and models of origin. *J. Petrol.* **2010**, *52*, 39–53. [CrossRef]
10. Loiselle, M.C.; Wones, D.R. Characteristics and origin of anorogenic granites. *Geol. Soc. Am. Abst. Prog.* **1979**, *11*, 468.
11. Anderson, J.L.; Morrison, J. Ilmenite, Magnetite, and peraluminous Mesoproterozoic Anorogenic granites of Laurentia as Baltica. *Lithos* **2005**, *80*, 45–60. [CrossRef]
12. Chappel, B.W.; White, A.J.R. Two contrasting granite types. *Pac. Ged.* **1974**, *8*, 173–174.
13. Anderson, J.L.; Bender, E.E. Nature and origin of Proterozoic A-type granitic magmatism in the southwestern United States of America. *Lithos* **1989**, *23*, 19–52. [CrossRef]
14. Streckeisen, A.L. Classification and nomenclature of igneous rocks. *Neus Jahrbuch für Mineralogie Abhandlungen* **1976**, *107*, 144–240.
15. Pietranik, A.B.; Hawkesworth, C.J.; Storey, C.D.; Kem, A.I.S.; Sircombe, K.N.; Whittehouse, M.J.; Bleeker, W. Episodic, mafic crust formation from 4.5 to 2.8 Ga: New evidence from detrital zircons, Slabe craton, Canada. *Geol. Soc. Am.* **2008**, *36*, 875–878. [CrossRef]
16. Kloosterman, J.B. Granites and rhyolites of São Lourenço: A volcano-plutonic complex in southern Amazonia. *Eng. Min. Met.* **1966**, *44*, 169–171.
17. Kloosterman, J.B. A tin province of the Nigerian type in southern Amazônia. In Proceedings of the Technical Conference on Tin, 2, London, UK, 2 February 1968; pp. 381–400.
18. Bettencourt, J.S.; Tosdal, R.M.; Leite, W.B., Jr.; Payolla, L. The Rapakivi Granites of Rondônia. Tin Province and Associated Mineralization. In Proceedings of the Symposium Rapakivi Granites and Related Rocks, 6, Belém, Brazil, 2–5 August 1995; pp. 5–16.
19. Bettencourt, J.S.; Tosdal, R.M.; Leite, W.B., Jr.; Payolla, B.L. Mesoproterozoic rapakivi granites of the Rondônia Tin Province, southwestern border of the Amazonian craton, Brazil—I. Reconnaissance U-Pb geochronology and regional implications. *Precambrian Res.* **1999**, *95*, 41–67. [CrossRef]
20. Dall'Agnol, R.; Costi, H.T.; Leite, A.A.S.; Magalhães, M.S.d.; Teixeira, N.P. Rapakivi granites from Brazil and adjacente áreas. *Precambrian Res.* **1999**, *95*, 9–39. [CrossRef]
21. Almeida, F.F.; Hasui, Y.; Brito Neves, B.B.; Fuck, R.A. *As províncias estruturais do Brasil*; VIII Simp. GeoI. Nord.: Campina Grande, PB, Brazil, 1977; pp. 363–391.
22. Whalen, J.B.; Curffi, K.L.; Chappel, B.W. A-Type granites: Geochemical characteristics, discrimination, and petrogenesis. *Contrib. Meneral. Petrol.* **1987**, *95*, 407–419. [CrossRef]
23. Bonn, B. A-type Granites and related Rocks: Evolution of a concept, problems, and prospects. *Lithos* **2007**, *97*, 1–29. [CrossRef]
24. Állegre, C. *Géologie Isotopique*; Editora Belin: Paris, France, 2005; 285p.
25. Dall'Agnol, R.; Oliveira, D.C. Oxidized, magnetite-series, rapakivi-type granites of Carajás, Brasil: Implications for classification and petrogenesis of A-type granites. *Lithos* **2007**, *93*, 215–233. [CrossRef]
26. Haapala, I.; Ramo, O. Rapakivi granites and related rocks: An introduction. *Precambrian Res.* **1995**, *95*, 1–7. [CrossRef]

27. Bettencourt, J.S.; Leite, W.B., Jr.; Payolla, B.L.; Scandolara, J.E.; Muzzolon, R.; Viana, J.A.J. The rapakivi granites of the Rondônia Tin Province, Northern Brazil. In Proceedings of the International Symposium on Granites and Associated Mineralizations (ISGAM II), Salvador, Brazil, 21–31 January 1997.
28. Bettencourt, J.S.; Muzzolon, R.; Payolla, B.L.; Daluigna, L.G.; Pinho, O.G. Depósitos estaníferos secundários da região central de Rondônia. In *Depósitos Minerais do Brasil*; Schobbenhaus, C., Coelho, C.E.S., Eds.; DNPM: Rio de Janeiro, Brazil, 1988; Volume III, pp. 213–241.
29. Bettencourt, J.S.; Dall'Agnol, R. The Rondonian tin-bearing anorogenic granites, and associated mineralization. In Proceedings of the International Symposium on Granites and Associated Mineralizations, Salvador, Brazil, 21–31 January 1997; Nobrega, A., McReath, I., Eds.; Superintendência de Geologia e Recursos Minerais: Rio de Janeiro, Brazil, 1987; Volume 1, pp. 1–144.
30. Vorma, A. On the petrochemistry of rapakivi granites with special reference to the Laitila massif, southwestern Finland. *Bull. Geol. Surv. Finl.* **1976**, *285*, 98.
31. Larin, A.M. Rapakivi granites in the geological history of the earth. Part 1, magmatic associations with rapakivi granites: Age, geochemistry, and tectonic setting. *Strat. Geol. Correl.* **2009**, *17*, 235–258. [CrossRef]
32. Bizzi, L.A.; Schobbenhaus, C.; Vidotti, R.M.; Gonçalves, J.H. *Geologia, Geotectônica e Recursos Minerais do Brasil*; CPRM: Sao Paulo, Brazil, 2003; pp. 169–195.
33. Colombo, F.; Lira, R.; Miner, R.E. Mineralogical Characterization of topaz from miarolitic pegmatites and w-bearing greisen in the A-Type El Portezuelo granite, Papachacra (Catamarca Province). *Rev. Assoc. Geol. Argent.* **2009**, *64*, 194–200.
34. CPRM, Serviço Geologico do Brasil. *Geologia e Recursos Minerais do Estado de Rondônia—Sistema de Informações Geográficas—SIG. Programa Geologia do Brasil—Integração, Atualização e Difusão de Dados da Geologia do Brasil*; Mapas Geológicos Estaduais Escala 1:1.000; Programa Geologia do Brasil: Porto Velho, Brazil, 2007; pp. 13, 45–46.
35. Coutinho, M.G.N. Província Mineral do Tapajós: Geologia, metalogenia e mapa previsional para Ouro Preto em Sig. In *CPRM, Geologia e Recursos Minerais do estado de Rondônia*; Programa Geologia do Brasil: Porto Velho, Brazil, 2007; pp. 13, 45, 68–79.
36. Dall'Agnol, R.; Teixeira, N.P.; Ramo, O.T.; Moura, C.A.V.; Macambira, M.J.B.; de Oliveira, D.C. Petrogenesis of the Paleoproterozoic rapakivi, A-type granites of the Archean Carajás Metallogenic Province, Brazil. *Lithos* **2005**, *80*, 101–129. [CrossRef]
37. Dias, C.A.T. Geologia e Mineralogia de Pegmatito Mineralizado em Estanho e Metais Associados (Nb, Ta, Zn, Cu e Pb), Mina Bom Futuro—RO. Rio Claro–SP. Master's Thesis, Universidade Estadual Paulista, Sao Paulo, Brazil, 2012; 89p.
38. Geraldes, M.C.; Nogueira, C.C. Rondônia Tin Province, SW Amazonian Craton Revised: Geochronologiy, Magmatic Processes and Tectonic Setting. *SGA, Simp. Geologia da Amazônia*. 2013. Available online: https://sbg-no.org.br/arquivos/BASES/SGA%2013.pdf (accessed on 1 August 2022).
39. Santos, J.O.S.; Rizzotto, G.J.; Potter, P.E.; McNauughton, N.J.; Matos, R.S.; Hartmann, L.A.; Chemale, F., Jr.; Quadros, M.E.S. Age and autochthonous evolution of the Sunsás Orogen in west Amazon Craton based on mapping and U-Pb geochronology. *Precambrian Res.* **2008**, *165*, 120–152. [CrossRef]
40. Almeida, F.F.; HasuiI, Y.; Brito Neves, B.B. *The Upper Precambrian of South America*; Boletim, I.G., Ed.; Instituto de Geociências da USP: Sao Paulo, Brazil, 1976; Volume 7, pp. 45–80.
41. Cordani, U.G.; Tassinari, C.C.G.; Teixeira, W.; Basei, M.A.S.; Kawashita, K. Evolução tectônica da Amazônia com base nos dados geocronológicos. In *Congresso Geológico Chi-leno, 2., Arica*; Instituto de Investigaciones Geológicas: Santiago, Chile, 1979; pp. 137–148.
42. Teixeira, W.; Tassinari, C.C.; Cordani, U.; Kawashita, K. A review of the geochronology of the Amazonian Craton: Tectonic implications. *Precambrian Res.* **1989**, *42*, 213–227. [CrossRef]
43. Tassinari, C.C.G. O Mapa Geocronológico do Cráton Amazônico no Brasil: Revisão dos Dados Isotópicos. Master's Thesis, Universidade de São Paulo, São Paulo, Brazil, 1996; 139p.
44. Sadowiski, G.R.; Bettencourt, J.S. Mesoproterozoic tectonic correlations between eastern Laurentia and the western border of the Amazonian Craton. *Precambrian Res.* **1996**, *76*, 213–227. [CrossRef]
45. Tassinari, C.C.G.; Macambira, M. Geochronological Provinces of the Amazonian Craton. *Episodes* **1999**, *22*, 174–182. [CrossRef] [PubMed]
46. Scandollara, J.E.; Fuck, R.A.; Dall'Agnol, R.; Dantas, E.L. Geochemistry and origin of the early Mesoproterozoic mangerite-charnokite-rapakivi granite association of the Serra da Providência suíte and associated gabbros, central-eastern Rondônia, SW Amazonian Craton, Brasil. *J. South Am. Earth Sci.* **2013**, *45*, 166–193. [CrossRef]
47. Scandollara, J.E.; Rizzotto, G.J.; de Amorim, J.L.; Bahia, R.B.C.; Quadros, M.L.; da Silva, C.R. *Geological Map of Rondônia*; CPRM: Porto Velho, Brazil, 1999; Escala:1:1000 000.
48. Quadros, M.L.d.E.S.; Rizzoto, G.J. (Eds.) *Geologia e Recursos Minerais do Estado de Rondônia: Sistema de Informações Geográficas—SIG: Texto Explicativo do Mapa Geológico e de Recursos Minerais do Estado de Rondônia*; CPRM: Porto Velho, Brazil, 2007; 153p.
49. Isotta, C.A.L.; Carneiro, J.M.; Kato, H.T.; Barros, R.J.L. *Projeto Província Estanífera de Rondôni*; DNPM/CPRM: Porto Velho, Brazil, 1978; Volumes 1–3.
50. Queiroz, L.A.V.; Macambira, M.; Nogueira, C.C.; Quadros, M.L.E.S. Estudos litogeoquímicos, isotópicos e petrográficos da Suíte Intrusiva Alto Candeias. *Contribuições a Geologia da Amazonia* **2010**, *10*, 285–307.
51. Geraldes, M.C.; Teixeira, W.; Heilbron, M. Lithospheric versus asthenospheric source of the SW Amazonian craton A-types granites: The role of the Paleo- and Mesoproterozoic accretionary belts for their coeval continental suites. *Episodes* **2004**, *27*, 185–189. [CrossRef] [PubMed]

52. Debowski, B.P.; dos Santos, A.C.; Santos, W.H.; Geraldes, M.C. Petrograia e Litogeoquímica dos Maciços Massangana, São Carlos e Caritianas Pertencentes aos Granitos mais Jovens da Província Estanífera de Rondônia. *Anuário Inst. Geoci.* **2019**, *41*, 395–412. [CrossRef]
53. Payolla, B.L. As Rochas Graníticas e Sieníticas das Cachoeiras Teotônio e Santo Antônio, Rio Madeira, Porto Velho, Rondônia: Geologia, Petrografia e Geoquímica. Master's Thesis, Universidade de Brasília, Asa Norte, Brazil, 1994; 145p.
54. Santos, P.C.M., Jr. Metalogênese do Depósito de Estanho Liberdade, Campo Novo de Rondônia—RO. Brasília—DF. Master's Thesis, Universidade de Brasília, Asa Norte, Brazil, 2015; 102p.
55. Souza, V.S.; Botelho, N.F.; Dantas, E.L.; Laux, J.H. Geoquímica e geologia isotópica (Sm-Nd e U-Pb) de magmatismo traquítico no depósito de estanho do Bom Futuro (RO). *Rev. Bras. Geoci.* **2007**, *37*, 660–667. [CrossRef]
56. Sparremberger, I. Evolução da Mineralização Primária Estanífera Associada ao Maciço Granítico Santa Bárbara, Rondônia. Ph.D. Thesis, Universidade de São Paulo, Sao Paulom, Brazil, 2003; 254p.
57. Debowski, B.; Alves, M.; dos Santos, A.C.; Tavares, A.D., Jr.; Geraldes, M. Contribution to the understanding of the Rondonia Tin Province granites (SW Amazonian Craton) origin using U-Pb and Lu-Hf in zircon by LA-ICPMS: Implications to A-type granite genesis. *J. Geol. Surv. Braz.* **2019**, *2*, 151–164. [CrossRef]
58. Nogueira, C.C.; Geraldes, M.C.; Saar de Almeda, B.; Debowski, B. Provincia Estanifera de Rondoia: Caracterização e distribuição temporal da mineralização. In *Contribuições a Geologia da Amazonia*; Sociedade Brasileira de Geologia: Sao Paulo, Brazil, 2015; Volume 9, pp. 393–408.
59. Romaninni, S.J. Geologia e Geoquímica do Complexo Granitóide de Massangana e Sua Relação com as Mineralizações de Estanho. Master's Thesis, Curso de Pós-Graduação em geociências, Salvador, Brazil, 1982; 85p.
60. Geraldes, M.C. *Introdução à Geocronologia*; Sociedade Brasileira de Geociências: São Paulo, Brazil, 2010; 137p.
61. Faure, G. *Principles of Isotope Geology*, 2nd ed.; John Wiley & Sons: Hoboken, NJ, USA, 1986; 589p.
62. Geraldes, M.C.; Teixeira, W.; Valladares, C. Contribuição ao estudo do magmatismo Paleo e Mesoproterozóico do SW do Craton Amazônico através da aplicação de isótopos estáveis de O, H e S. *Acta Amazonica (Impresso)* **2008**, *38*, 159–167. [CrossRef]
63. Geraldes, M.C.; Bettencourt, J.S.; Teixeira, W.; Matos, J.B. Geochemistry and isotopic constraints on the origin of the mesoproterozoic Rio Branco anorogenic plutonic suite, SW of Amazonian craton, Brazil: High heat flow and crustal extension behind the Santa Helena arc? *J. South Am. Earth Sci.* **2004**, *17*, 195–204. [CrossRef]
64. Nascimento, T.M.F. Depósito de W-Sn Igarapé-Manteiga: Geologia e Metalogênese. Master's Thesis, Universidade Federal do Amazônico, Manaus, Brazil, 2010.
65. Rizzotto, G.J.; Scandolara, J.E.; Silva, C.R.; Dall'Agnol, R.; Bettencort, J.S.; Morais, P.R. Geology and preliminary geochemistry of the middle proterozoic Serra da Providência rapakivi granite-Rondonia, Brazil. In Proceedings of the Symposium on Rapakivi Granites and Related Rocks, Belem, Brazil, 2–5 August 1995; pp. 5–16.
66. Villeneuve, M.; Wazi, N.; Kalikone, C.; Gärtner, A. A Review of the G4 "Tin Granites" and Associated Mineral Occurrences in the Kivu Belt (Eastern Democratic Republic of the Congo) and Their Relationships with the Last Kibaran Tectono-Thermal Events. *Minerals* **2022**, *12*, 737. [CrossRef]
67. O'Connor, J.T. A classification for quartz-rich igneous rocks based on feldspar ratios. *US Geol. Surv.* **1965**, *525B*, B79–B84.
68. Pearce, J.A.; Harris, N.B.W.; Tindle, A.G. Trace Element Discrimination Diagrams for the Tectonic Interpretation of Granitic Rocks. *J. Pet.* **1984**, *25*, 956–983. [CrossRef]
69. Black, R.; Lameyre, J.; Bonin, B. The structural setting of alkaline complexes. *J. Afr. Earth Sci.* **1985**, *3*, 5–16. [CrossRef]
70. Griffin, W.L.; Belousova, E.; Walters, S.G.; O'Reilly, S.Y. Archaean and Proterozoic crustal evolution in the Eastern Succession of the Mt Isa district, Australia: U—Pb and Hf-isotope studies of detrital zircons. *Aust. J. Earth Sci.* **2006**, *53*, 125–149. [CrossRef]
71. Patchett, P.J.; Kouvo, O.; Hedge, C.E.; Tatsumoto, M. Evolution of continental crust and mantle heterogeneity: Evidence from Hf isotopes. *Contrib. Mineral. Petrol.* **1981**, *78*, 279–297. [CrossRef]
72. Vervoort, J. Lu-Hf Dating: The Lu-Hf Isotope System. In *Encyclopedia of Scientific Dating Methods*; Rink, W., Thompson, J., Eds.; Springer: Dordrecht, The Netherlands, 2014. [CrossRef]
73. Griffin, W.L.; Pearson, N.J.; Belousova, E.; Jackson, S.E.; O'Reilly, S.Y.; Van Achterberg, E.; Shee, S.R. The Hf isotope composition of cratonic mantle: LAM-MC-ICPMS analysis of zircon megacrysts in kimberlites. *Geochim. Cosmochim. Acta* **2000**, *64*, 133–147. [CrossRef]
74. Gerdes, A.; Zeh, A. Combined U-Pb and Hf isotope LA-(MC)-ICP-MS analyses of detrital zircons: Comparison with SHRIMP and new constraints for the provenance and age of an Armorican metasediment in Central Germany. *Earth Planet Sci. Lett.* **2006**, *249*, 47–61. [CrossRef]
75. Belousova, E.; Griffin, W.L.; O'Reilly, S.Y. Zircon Crystal Morphology, Trace Element Signatures and Hf Isotope Composition as a Tool for Petrogenetic Modelling: Examples from Eastern Australian Granitoids. *J. Pet.* **2005**, *47*, 329–353. [CrossRef]
76. Rizzotto, G.J.; Quadros, M.L. DO E. S. Geologia da Amazonia Ocidental. In SBG Cong. Brasileiro de Geologia, 42, Araxa. Anais. Araxa: SBG-Nucleo Minas Gerais. 1 CD-Rom, 2014.
77. Pichavant, M.; Manning, D. Petrogenesis of tourmaline granites and topaz granites; the contribution of experimental data. *Phys. Earth Planet. Inter.* **1984**, *35*, 31–50. [CrossRef]
78. Collins, W.J.; Beams, S.D.; White, A.J.R.; Chappell, B.W. Nature and origin of A-type granites with particular reference to southeastern Australia. *Contrib. Miner. Pet.* **1982**, *80*, 189–200. [CrossRef]